A Study of Bianisotropy in Split Ring Structures made with Graphene and Gold

A THESIS
SUBMITTED TO THE FACULTY OF THE GRADUATE SCHOOL
OF THE UNIVERSITY OF MINNESOTA
BY

Amartya Kumar Ghosh

IN PARTIAL FULFILLMENT OF THE REQUIREMENTS
FOR THE DEGREE OF
MASTER OF SCIENCE

Dr Anand Gopinath

December, 2016

Acknowledgements

There are many people that have earned my gratitude for their contribution to my time in the graduate school, here at University of Minnesota-Twin Cities. Firstly I would like to thank my main advisor Dr Anand Gopinath for giving me the opportunity to work under him. It was a great opportunity for me to exchange ideas with him and learning from him constant basis. Secondly I would like to thank Dr Tony Low, Dr Roberto Grassi for their supports and Dr Andrei Nemilentsau for helping me with the work. Thirdly my earnest gratitude goes to my other lab colleagues especially, Mr Eng Lee Hock, Mr Kaveh Khaliji and Mr Javad Ghasani for their time in giving me valuable suggestions from time to time.

Dedication

To those who held me up over the years- my parents, Mr Asim Ghosh and Mrs Silpi Ghosh and my other family members.

Abstract

An electromagnetic study of sub-wavelength structures made with graphene and gold is done with a concentration on the electro-magnetic coupling of these structures. The aim of the thesis is to analyze the reflection and transmission coefficients from the numerical simulations done with the help of COMSOL. Then homogenize these periodic array of structures for varying thicknesses so that it behaves as a continuous medium in the long wavelength limit. The next goal is to retrieve the effective electromagnetic parameters like the permittivity, permeability and refractive index from this homogenized structure. This will lead to tuning the electromagnetic properties according to the requirements-the property which is not available in naturally occurring materials, because the electrical or magnetic properties in naturally occurring materials are fixed. This new kind of material is defined as the metamaterial. The effective parameters of these materials are dependent on the properties of the basic materials with which the periodic array of structures are made - for example, it will be seen later how the effective properties is different when graphene is used instead of gold. The approach here is to use a normally incident wave on these periodic arrangement of graphene or gold structures and extract the scattering coefficients. Then invert these reflection and transmission data using basic Maxwell's equations to determine the refractive index and the impedance of the multilayered slab. From here the self consistent equations, the permittivity and permeability is determined. When the metamaterial is made with graphene it is found that the continuous slab behaves as an optical non magnetic material while with gold it behaves as a magnetic material. Some studies are also done on the dispersion of graphene nanoribbons and the electromagnetic modes associated with it.

Contents

Acknowledgements i

Dedication ii

Abstract iii

List of Tables vii

List of Figures viii

1 Introduction to Graphene: A Review of the Band Structure 1

1.1 Graphene Overview 1

1.2 Atomic Structure in Graphene 2

1.3 Derivation of the Band Structure 3

2 Graphene Conductivity Model 7

2.1 Introduction 7

2.2 Features 7

2.3 Local Conductivity Model using Boltzman Transport Equation 8

2.4 Drude Model from Finite Sized Kubo Formula 10

2.4.1 Comparison 11

3 Wave Propagation in Graphene 13

3.1 Basics 13

3.2 Maxwell's Equations 13

3.3 Analytical Approach 14

3.3.1 Coefficient Derivation 15
3.3.2 Numerical 16
3.3.3 Absorption for a suspended graphene layer 17

4 Graphene Nanoribbons: A study of the Electromagnetic Modes 20
4.1 Basic Idea of Nanoribbons 20
4.2 Basic Simulations and Analytical Calculations 21
4.3 Studies on Graphene Nanoribbons 22
4.4 Surface Plasmon Modes in Graphene Nanoribbons 23
4.4.1 Hybridized Surface Plasmon Modes in Graphene Nanoribbons . . 25

5 Metamaterials based on Split Ring Resonators and Gold 28
5.1 Introduction 28
5.1.1 Brief History of Metamaterials 29
5.1.2 Meaning of negative index 29
5.1.3 The basic physics of Metamaterials 30
5.2 The Split Ring Resonators: The Electromagnetic Response 32
5.2.1 Deriving the field equation inside 36
5.2.2 Parameter Retrieval from the S-parameters 40
5.2.3 Maxwell's equation in the metamaterial slab 41
5.2.4 Parameter Retrieval: Using the Boundary conditions 42
5.3 Application 46
5.3.1 Problems with matching Analytical and Simulational Caulculations 46
5.3.2 Application to a Lossy Slab 47
5.3.3 Application to the Graphene Split Ring Resonators 48
5.3.4 Application to Gold Nanostructures 49

6 Summary 53
6.1 Conclusion 53
6.2 Future Work 54

References 55

Appendix A. Supplemental Calculations **60**
A.1 The Lossy Slab 60
A.2 Graphene Nanoribbons Surface Plasmons 64
A.3 Finding f(k) - the Structural Factor 65
A.4 Finding the elements of the Hamiltonian Matrix 66

List of Tables

List of Figures

1.1 (a)The unit cell in the hexagonal lattice in real space formed by the sides a_1 and a_2.(b)The lattice in reciprocal space 2
1.2 The energy band diagram 6
2.1 (a)Real part of conductivity of Kubo vs Drude 12
3.1 The Geometry 14
3.2 Absorption Plot 18
3.3 (a) Reflection plot comparison for various incident angles (b) Transmission comparison for various incident angles 19
4.1 Transmission, Reflection and Absorption coefficient of a graphene sheet on SiO2 21
4.2 Graphene Nanoribbons Geometry and the corresponding Absorption Spectra 22
4.3 Comparison between the the Analytical and Simulational Model 25
4.4 The Surface Plasmon Modes 26
4.5 The Propagation Length of Surface Plasmon Modes 27
5.1 a)Right Handed Material b) Left Handed Materials 30
5.2 Metamaterials classification. Figure taken from [33] 31
5.3 SRR Geometry and the wave configuration 32
5.4 Response by varying the width of the gap same as controlling the sector angle: The blue line shows the relative absorption difference when light is incident from the top port and from the bottom port. 33
5.5 Response by varying the radius of the sector: The blue line shows the relative absorption difference when light is incident from the top port and from the bottom port. 34

5.6 Response by varying the angle of incidence: The blue line shows the relative absorption difference when light is incident from the top port and from the bottom port. 35
5.7 The geometry of the SRR structure and the E,H,k convention 36
5.8 The geometry of the SRR structure and the E,H,k convention 40
5.9 The homogenized material 43
5.10 The electric and magnetic response before the corrections 46
5.11 The geometry and the EM comfiguration of the Lossy Slab 48
5.12 Analytical and numerical comparison of the Reflectance and Transmission coefficient 49
5.13 The Phase Difference 50
5.14 The Effective Parameter Derivations 51
5.15 The Reflectance, Transmittance and the effective Parameters for Gold . 52

Chapter 1

Introduction to Graphene: A Review of the Band Structure

1.1 Graphene Overview

Graphene is a single atom thick layer of carbon atoms, first synthesized by peeling off bulk graphite, in 2004, by Andre Geim and his research group at the University of Manchester [1] .It is a two dimensional allotrope of carbon [5] tightly packed in a honeycomb lattice like structure and is the thinnest possible material known to exist. But theoretical works, like calculating the electronic transport properties of the 2D graphite system, had started almost half a century ago [3, 4]. It was never thought then, that there can be a possibility to obtain free standing 2D structures, because it was seen that the thin film atomic layers of most elements(around 12-13 atomic layers thin) are thermodynamically very unstable [2] due to the huge decrease in melting point at the room temperatures. Moreover theoretically it was shown by Mermin [6] that isolated 1D or 2D structures are not possible to produce due to formation of dislocations in these structures. Therefore when graphene was discovered in 2004 and it was shown to be a stable material at room temperatures, extensive research followed which led to numerous papers in the following years. In this chapter, the electronic configuration of graphene will be briefly discussed and then its band structure will be derived.

1.2 Atomic Structure in Graphene

In graphene, the three sp electrons of the carbon atoms form hybrid covalent bonds with the neighboring atoms while the fourth one, which resides in the p_z orbital, moves freely across the plane of the graphene sheet. This electron is responsible for mobility and charge transport properties in graphene. When covalent bonds are formed, the wavefunctions of the neighboring atoms overlap in such a way that the energy gain is maximum. If the wave function analysis is done by solving the Schrodinger equations for maximum overlap(which is necessary to have maximum energy), it can be shown that the orbits which have a maxima in one plane is separated by 120 degrees. These bonds are known as the σ bonds while the bonds formed between the p_z orbital electrons is defined as the π bonds. The Bravais lattice in the honeycomb crystal lattice of graphene is triangular as shown in the following Figure 1.1. The honeycomb lattice structure contains two atoms per unit cell.

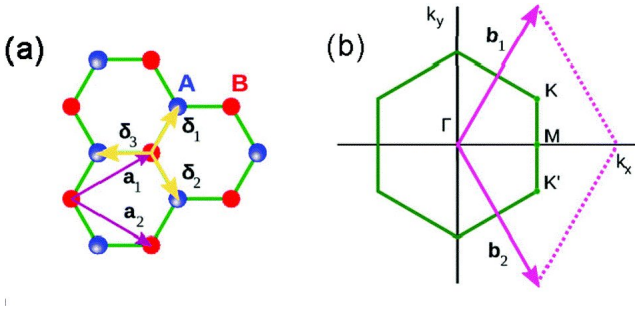

Figure 1.1: (a)The unit cell in the hexagonal lattice in real space formed by the sides a_1 and a_2.(b)The lattice in reciprocal space

The Figure 1.1 shows the unit cell in the hexagonal layer formed by the sides $\vec{a_1}$ and $\vec{a_2}$. By simple geometry it can be shown that the magnitude of these vectors is given as $|\vec{a_1}| = |\vec{a_2}| = \sqrt{3}l = 2.46°$ where l is the bond length of the C-C atom. The primitive vectors $\vec{a_1}$ and $\vec{a_2}$ can be also be written in column matrices as:-

$$\vec{a_1} = a \begin{pmatrix} \frac{\sqrt{3}}{2} \\ \frac{1}{2} \\ 0 \end{pmatrix}$$

$\vec{a_2} = a \begin{pmatrix} \frac{\sqrt{3}}{2} \\ \frac{-1}{2} \\ 0 \end{pmatrix}$ and $\vec{a_3} = \begin{pmatrix} 0 \\ 0 \\ 1 \end{pmatrix}$

The vector $\vec{a_3}$ is taken to find the reciprocal lattice vectors.

Each atom is surrounded by three nearest neighboring atoms with distances given by $\delta_1 = \frac{a}{2}(1, \sqrt{3}), \delta_2 = \frac{a}{2}(1, -\sqrt{3}), \delta_3 = a(-1, 0)$

Now the triangular reciprocal lattice space vectors can be found by using the relation

$$\vec{b_j} = 2\Pi \frac{\vec{a_k} \times \vec{a_l}}{\vec{a_j} \cdot (\vec{a_k} \times \vec{a_l})}$$

where $\vec{b_1} = 2\Pi \frac{\vec{a_2} \times \vec{a_3}}{\vec{a_1} \cdot (\vec{a_2} \times \vec{a_3})} = \frac{2\Pi}{a} \begin{pmatrix} \frac{1}{\sqrt{3}} \\ 1 \end{pmatrix}$ and $\vec{b_2} = 2\Pi \frac{\vec{a_3} \times \vec{a_1}}{\vec{a_2} \cdot (\vec{a_3} \times \vec{a_1})} = \frac{2\Pi}{a} \begin{pmatrix} \frac{1}{\sqrt{3}} \\ -1 \end{pmatrix}$

Figure 1.1b represents the geometry of the first Brillouin zone in the reciprocal space. κ and κ' are the two inequivalent corners or valley in this hexagonal space, known as the Dirac points. It is not possible to travel between these two adjacent points by translational symmetry of the reciprocal lattice vectors. This is the reason these Dirac points gives rise to chirality in carrier dynamics.

The charge carriers in graphene display some unique characteristic which makes graphene a more attractive research material. The dynamics cannot be defined by Schrodinger equation,rather it exhibits relativistic particle behavior and thus follow the Dirac equations [7] . When interacting with the periodic potential of lattice structure the electrons gives rise to new quasiparticles called massless Dirac fermions. The formulation of these Dirac fermions can be derived using the tight binding approximation for graphene.

1.3 Derivation of the Band Structure

Following the derivation from [5] and taking only the nearest neighbor coupling the Dirac Hamiltonian matrix is given by

$$H = \begin{bmatrix} < \Phi_A|H|\Phi_A > & < \Phi_A|H|\Phi_B > \\ < \Phi_B|H|\Phi_A > & < \Phi_B|H|\Phi_B > \end{bmatrix} \tag{1.1}$$

where $|\Phi_A|>$and$|\Phi_B>$ are the wavefunctions of the p_z orbital electrons of the atoms, A and B in the unit cell of Figure 1.1. The matrix can be simplified to

$$H = \begin{bmatrix} \epsilon_{2p} & tf(\vec{k}) \\ tf(\vec{k})^* & \epsilon_{2p} \end{bmatrix} \tag{1.2}$$

The simplification process and each of the terms are explained as below:-

ϵ_{2p} is the energy of the p_z orbital overlap between the atoms of the two neighboring unit cells given as $<\Phi_A|H|\Phi_A>=\frac{1}{N}\sum_{R=R^{'}}<\Phi_A(r-R)|H|\Phi_A(r-R)>$.

This term represents the summation over all the unit cells across the lattice that takes this same value, ϵ_{2p}. In a similar argument the other diagonal element, $<\Phi_B|H|\Phi_B>$ can also be taken as ϵ_{2p} because graphene is considered to be intrinsic.

The cross term represents the overlap of the p_z electrons of the two sites, A and B of the same unit cell. From Figure 1.1 it can be noticed that if one considers the overlap from site A, then three nearest possible directions are there to overlap($\vec{\delta_1}$,$\vec{\delta_2}$ and $\vec{\delta_3}$),which is given by total 3 couplings as follows:-

$<\Phi_A|H|\Phi_B>=\frac{1}{N}\sum_{R=R^{'}}\{<\Phi_A(r-R)|H|\Phi_B(r-R)>\exp(i\cdot\vec{k}\cdot\vec{\delta_1})+$

$<\Phi_A(r-R)|H|\Phi_B(r-R)>\exp(i\cdot\vec{k}\cdot\vec{\delta_2})+$

$<\Phi_A(r-R)|H|\Phi_B(r-R)>\exp(i\cdot\vec{k}\cdot\vec{\delta_3})\}$

$=t[\exp(i\cdot\vec{k}\cdot\vec{\delta_1})+\exp(i\cdot\vec{k}\cdot\vec{\delta_2})+\exp(i\cdot\vec{k}\cdot\vec{\delta_3})]=tf(k)$,where f(k) is known as the structural factor which is responsible for giving the dispersion in graphene. The next step is to find this dispersion relation. The Hamiltonian can be found at the vicinity of the Dirac points $\vec{\kappa}$ by replacing $\vec{k}$ in equation1.3 as $\vec{k}=\vec{\kappa}+\vec{q}$ where q has a very small magnitude with respect to κ. Now using the Taylor expansion and neglecting the higher order terms, the structural factor becomes

$f(\vec{q})=f(\vec{\kappa})+\vec{q}\nabla_{\vec{\kappa}}f(\vec{k})$

It can be shown that $f(\vec{\kappa})=0$[1] . The physical significance of $f(\kappa)$ being zero at the corner of the Brillouin zone is that the two points of the Brillouin zone cannot be connected by the reciprocal lattice vector.

The second term in the expansion, $\vec{q}\nabla_{\vec{\kappa}}f(\vec{k})$,can be simplified to[2] $\frac{3l}{2}(q_x-iq_y)\exp(i\theta)$

[1] Appendix A.3
[2] Appendix A.4

Therefore the Hamiltonian becomes

$$H = \begin{bmatrix} \epsilon_{2p} & \frac{3lt}{2}(q_x - iq_y)exp(i\theta) \\ \frac{3lt}{2}(q_x + iq_y)exp(-i\theta) & \epsilon_{2p} \end{bmatrix} \tag{1.3}$$

which is equal to

$$\begin{bmatrix} \epsilon_{2p} & \hbar v_F(q_x - iq_y)exp(i\theta) \\ \hbar v_F(q_x + iq_y)exp(-i\theta) & \epsilon_{2p} \end{bmatrix}$$

where v_F is known as the Fermi velocity[3] Now by using the unitary transformation one can get rid of the $exp(i\theta)$ term and the Dirac Hamiltonian matrix can simply be given by

$$H = \begin{bmatrix} \epsilon_{2p} & \hbar v_F(q_x - iq_y) \\ \hbar v_F(q_x + iq_y) & \epsilon_{2p} \end{bmatrix} \tag{1.4}$$

=

$$\hbar v_F[q_x\sigma_x + q_y\sigma_y] = \hbar v_F(\vec{q} \cdot \sigma)] \tag{1.5}$$

σ_x and σ_y are the Pauli spin matrices[4] , given by

$$\sigma_x = \begin{pmatrix} 0 & 1 \\ 1 & 0 \end{pmatrix}$$

and

$$\sigma_y = \begin{pmatrix} 0 & -i \\ i & 0 \end{pmatrix}$$

Thus from the Schrodinger equation, $H\psi = E\psi$, the resulting eigen values are $E = \pm\hbar v_F q$ showing a linear dispersion relation of graphene near the vicinity of the Dirac points describing massless chiral quasiparticle behavior as given in Figure 1.2. The dispersion is same as that of visible light, except that the speed.v_F of the particles in graphene is 300 times smaller.

[3] dimension of $[\frac{lt}{\hbar}]$ is that of velocity

[4] We have considered that $\epsilon_{2p} = 0$ since this term is independent of k and thus does not really contribute to the dispersion relation

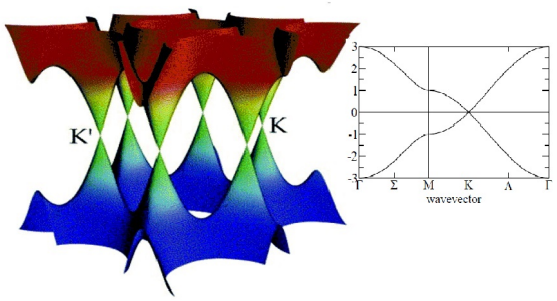

Figure 1.2: The energy band diagram

The two atoms per unit cell results in two conical points per Brillouin zone where the intersection of the band occurs.

The formation of these conical sections of the energy spectrum intersecting at zero E shows that graphene is indeed a zero band gap semiconductor with lesser amount of density of states.

Again using the eigen value equation we can find the normalized wave functions for the two sublattice points A and B as

$$\psi = \frac{1}{\sqrt{2}} \begin{bmatrix} \exp(i\theta) \\ \exp(-i\theta) \end{bmatrix}$$

Therefore from Figure 1.2 it can be seen that the energy tends to go to 0 near the Brillouin zone corners while at other areas in the K-space $E(k) \neq 0$ which means the dispersion is no more linear and there is a split in the band structure as shown in Figure 1.2.

Chapter 2

Graphene Conductivity Model

2.1 Introduction

Conductance G of a large macroscopic conductor can be defined as the inverse of resistance which is directly proportional to the cross sectional area A and the length L of the conductor, given as G=σA/L (Ohm's law), where σ is known as the conductivity of the material.

The measurement of this conductivity becomes a challenge when the material length is scaled down, for example in the nano regime. But with the development of nanoelectronics, it has been possible to build nanotransistors which finally enabled us to calculate the conductivity in this scale experimentally. In this chapter, the conductivity model which has been used in the subsequent chapters for measuring optical properties in various nano structures will be discussed and derived from two different approaches- the Boltzman transport equation approach and from the random phase approximation approach.

2.2 Features

The conductivity in graphene has two important characteristics as follows:

1)the minimum conductivity in graphene never falls below a certain minimum value, which is equal to $e^2/\pi h$ even at the charge neutrality point [8, 9] and

2) a linear increase in σ with charge carrier density,n away from the Dirac point

[11] which can be explained in the framework of Boltzmann Transport theory [12] for Coulomb scatterers, since Boltzmann theory does not apply near the vicinity of Dirac points.

2.3 Local Conductivity Model using Boltzman Transport Equation

[10] Consider f_0(**r**,**k**,t) as the non equilibrium distribution function(ie the probability of finding an electron at position **r** at time t with quasi momentum $\hbar$**k**). Now if a perturbation,f_1, is applied to the system (which can be anything like temperature gradient,or electric field or magnetic field,etc) one can track the motion of the electrons at time dt after the application of the perturbation. For example, in presence of an electric field and magnetic field, the force on the electron is given as $\mathbf{F}$(**r**,t)= $-\frac{e}{\hbar}$(**E**(**r**,t) + **v** x **B(r,**t))= $\hbar\frac{dk}{dt} = \frac{1}{\hbar}\frac{\partial\epsilon}{\partial k}$ where **v** is the electron velocity and $\epsilon = \hbar$vk is the eigen energy derived from Dirac Hamiltonian in Chapter 2.
Therefore after time dt the distribution function can be written as
f(**r**+**v**dt,**k**−$\frac{e}{\hbar}$dt,t+dt)(=f_0+f_1) which is same as f$_0$(**r**,**k**,t)+$\frac{\partial f}{\partial t}$|dt.
The term $\frac{\partial f}{\partial t}$|dt keeps a measure of the amount of scattering suffered by the electrons due to collisions. By using Taylor expansion the perturbed term can be expressed as below:-

$$\frac{\partial f}{\partial t} + \vec{v} \bigtriangledown_r f - \frac{e}{\hbar}(\vec{E}.\vec{\bigtriangledown}_k f) = \frac{f - f_0}{\tau} \tag{2.1}$$

where $\frac{\partial f}{\partial t}|dt$ is written using relaxation time approximation as

$$\frac{\partial f}{\partial t}|dt = \frac{f - f_0}{\tau}$$

Here we are considering that there is no spatial dispersion i.e the medium is homogeneous. Therefore the second term in the Equation(1), $\vec{v} \bigtriangledown_r f = 0$. Using this condition and taking f=f$_0$+f$_1$ as defined before we get,

$$\frac{\partial f_1}{\partial t} - \frac{e}{\hbar}(\vec{E}.\vec{\bigtriangledown}_k f_0) = -\frac{f_1}{\tau}$$
$$\implies \frac{\partial f_1}{\partial t} - \frac{e}{\hbar}(\vec{E}.\frac{\partial f_0}{\partial \epsilon}.\hbar\mathbf{v}) = -\frac{f_1}{\tau}$$

Now considering the applied perturbation to follow a time dependence as $\exp(i\omega t)$ and thus keeping only the first order terms the equation reduces to

$$j\omega f_1 - e(\vec{E}.\vec{v})\frac{\partial f_0}{\partial \epsilon} = -\frac{f_1}{\tau}$$

$$\Longrightarrow f_1 = \frac{e\frac{\partial f_0}{\partial \epsilon}(\vec{E}.\mathbf{v})}{j\omega + \frac{1}{\tau}} \tag{2.2}$$

which is the first order perturbation expression. Now we know the current density, $\mathbf{J}$ in the Fourier transform domain is given as

$$\mathbf{J}(\omega) = -\frac{2e}{(2\pi)^2}\iint \mathbf{v}(\mathbf{k}) f_1 d^2\mathbf{k}$$

$$\Rightarrow \mathbf{J}(\omega) = -\frac{2e}{(2\pi)^2}\iint \mathbf{v}(\mathbf{k})\frac{e\frac{\partial f_0}{\partial \epsilon}(\vec{E}.\mathbf{v})}{j\omega + \frac{1}{\tau}} d^2\mathbf{k} \tag{2.3}$$

since no current flows from the equilibrium distribution function. Therefore the conductivity,$\sigma(\omega)$ from the relation $\mathbf{J}$=$\sigma\mathbf{E}$ is given as

$$\sigma(\omega) = -\frac{2e}{(2\pi)^2}\iint \frac{e\frac{\partial f_0}{\partial \epsilon}(\mathbf{vv})}{\omega - j\frac{1}{\tau}} d^2\mathbf{k} \tag{2.4}$$

Some assumptions can be made here. Considering T = 0 Kelvin, -$\frac{\partial f_0}{\partial \epsilon}$ becomes a delta function, which is same as $\delta(E - E_F)$. Using the two relations and $\epsilon_F = \hbar v_F k_F$ and $n = \frac{k_F^2}{\pi}$, we get

$$\sigma(\omega) = \frac{e^2\tau n}{m(1 - j\omega\tau)} \tag{2.5}$$

This is the famous Drude model of local conductivity of an isotropic medium . Here we see that the conductivity is linearly variant with the carrier density, n. Another method to retrieve this same model can be derived from the finite sized Kubo conductivity formula based on random phase approximations.

2.4 Drude Model from Finite Sized Kubo Formula

From the random phase approximation [13] the conductivity model is given as in Equation 2.6 below. The derivation of this model is beyond the scope of this thesis. So the model is readily used as follows:-

$$\sigma_{\alpha\beta}(\omega) = -ie^2\hbar \sum_{kk'} \frac{f(\epsilon'_k) - f(\epsilon_k)}{\epsilon'_k - \epsilon_k} \frac{< k'|v_\alpha|k >< k'|v_\beta|k >}{\hbar(\omega + i/\tau) + \epsilon'_k - \epsilon_k} \tag{2.6}$$

where v_α and v_β are the Dirac Fermion velocity operators, f(E) is the Fermi-Dirac function, τ is the relaxation time of the particles and $|k>$ denotes an eigen state of the Dirac equation,

$$[-i\hbar v\sigma \bigtriangledown + V(r)]\psi = E\psi \tag{2.7}$$

Here it is considered that there is no magnetic field and hence the possibility of anomalous quantum Hall effect[ ] is absent in this situation. The isotropic medium for graphene has been studied here. Therefore the off diagonal terms in the conductivity tensor is zero that is, $\sigma_{xy} = 0 = \sigma_{yx}$, while only the diagonal elements will be present which are equal ($\sigma_{xx} = \sigma_{yy}$).
Now expressing all elements in terms of **k**, we get

$$v_\alpha = \frac{1}{\hbar} \bigtriangledown_{k_x} H$$

$$= \frac{1}{\hbar} \frac{\partial}{\partial k_x} \hbar v_F \begin{bmatrix} 0 & k_x - ik_y \\ k_x + ik_y & 0 \end{bmatrix}$$

$$= v_F \begin{bmatrix} 0 & 1 \\ 1 & 0 \end{bmatrix} \tag{2.8}$$

Therefore,we get $< k'|v_\alpha|k >= [v_F cos(\theta)] =< k'|v_\beta|k >$
Substituting these parameters in the equation 2.6, we get the isotropic conductivity

model as,

$$\sigma_{xx}(\omega) = -\frac{4ie^2\hbar}{(2\pi)^4}\int dk \int dk' \frac{f(\epsilon'_k) - f(\epsilon_k)}{(\epsilon'_k - \epsilon_k)} \frac{v_F^2 cos^2\theta}{\hbar(\omega + i/\tau) + \epsilon'_k - \epsilon_k}$$

$$= -\frac{4ie^2\hbar}{(2\pi)^4}\int dk \frac{f(\epsilon'_k) - f(\epsilon_k)}{(\epsilon'_k - \epsilon_k)} \frac{v_F^2 cos^2\theta}{\omega + i/\tau}$$

$$= -\frac{ie^2 v_F^2}{\omega + i/\tau}\int dk k(-\frac{\partial f}{\partial \epsilon})\int_0^{2\pi} cos^2\theta \, d\theta$$

$$= -\frac{ie^2}{\pi\hbar^2(\omega + i/\tau)}\int_0^{\infty} d\epsilon \epsilon(-\frac{\partial f}{\partial \epsilon})$$

Substituting T=0 Kelvin and replacing $\epsilon = \hbar v_F k_F$ and $n = k_F^2/\pi$, we get

$$\sigma_{xx}(\omega) = \frac{e^2\tau n}{m}\frac{1}{1 - i\omega\tau} \tag{2.9}$$

Again the well established Drude model for conductivity is derived from the random phase approximation. There are a few shortcomings in the Drude Model which sets in when the study spectrum is in the higher frequency range, for which one needs to use the Kubo conductivity model. A comparison between the two models is shown.

2.4.1 Comparison

The reliability of the Kubo conductivity model has been well established [10] for conventional non- relativistic two dimensional electron gases and metallic systems where the parabolic dispersion curve matches with the Drude conductivity model. But the Drude model is not ideal for visible frequency or far infrared regions. It can be shown by plotting the comparison between the two conductivity models as shown in the figure below.

The figure shows that the conventional Drude conductivity model fails for higher frequencies. For higher values of the denominator the σ goes to ~ 0 which is not true. The Kubo model addresses this part and accounts for the high frequency in the visible spectrum regime where the energy of the incident radiation is enough to cause transition to the conduction bands that is, interband transitions take place. Another important feature to note from the figure is that the conductivity goes to a minimum in the mid

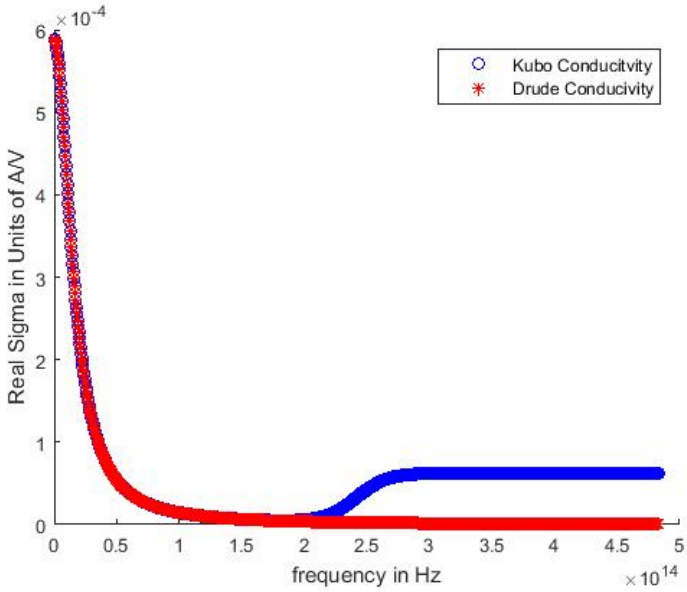

Figure 2.1: (a)Real part of conductivity of Kubo vs Drude

infrared regions-because the inter band transitions are absent here as the incident energy is less than twice the Fermi Energy, $2E_F$(where E_F is known as the Fermi energy) and hence Pauli blocking occurs. For the THz to the far infrared spectrum the two conductivity model overlaps. Most experimental results are obtained in this tunable part. This part can be explained in a very simple way. There is always some scattering present in the material which means there is relaxation time of the electrons. And hence applying Heisenberg's uncertainty principle, there is a splitting in the energy bands as well, therefore, the presence of intraband transitions. Hence there is some appreciable conductivity in this spectrum. All the studies in the subsequent chapters are done using the Kubo conductivity model.

Chapter 3

Wave Propagation in Graphene

3.1 Basics

In this chapter, electromagnetic wave propagation through a graphene layer is studied. Though this is a pretty straight forward study, but it is of particularly importance for the thesis as the following chapters are dedicated to wave propagation through more complicated structures. Moreover, due to unusual properties in graphene, the wave propagation through it is interesting as well. Using the complex surface conductivity model as derived in the previous chapter, an exact solution of the electromagnetic field is obtained. A comparative study is then done between the analytic results obtained from Maxwell's equations and the simulation results obtained from the finite element analysis Maxwell's solver -COMSOL.

3.2 Maxwell's Equations

The following are the four fundamental Maxwell's equations inside matter that are used in the analytical method. The first two laws states the Gauss's laws for electricity and magnetism while the third and the fourth are the Ampere's Laws and Faraday's laws respectively.

$$\nabla \times \mathbf{E} = -\frac{\partial \mathbf{B}}{\partial t} \tag{3.1}$$

$$\nabla \times \mathbf{H} = \mathbf{J}_f + \frac{\partial \mathbf{D}}{\partial t} \tag{3.2}$$

$$\nabla \mathbf{D} = \rho_f \tag{3.3}$$

$$\nabla \mathbf{B} = 0 \tag{3.4}$$

3.3 Analytical Approach

A monolayer of graphene is considered to be sandwiched between a dielectric substrate, for example, SiO_2 and air as shown in Figure 3.1. The permittivity of the subtrate is chosen to be ϵ_1 and the permittivity of the air medium above graphene is chosen to ϵ_2.

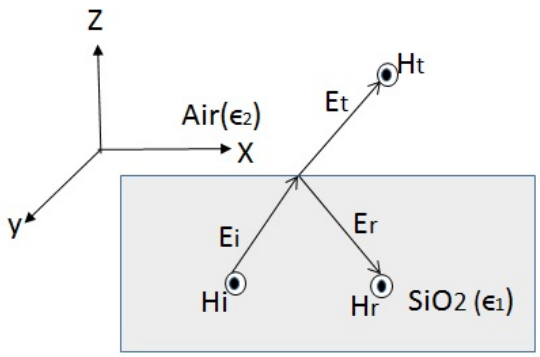

Figure 3.1: The Geometry

In this geometry two possible kinds of electromagnetic wave modes can exist-
i)the s-polarized mode or better known as the Transverse Electric(TE) mode(where the electric field of the incident electromagnetic is perpendicular to the plane of incidence

and

ii)the p-polarized or Transverse Magnetic(TM) modes, where the magnetic field is perpendicular to the plane of incidence.

Here the TM mode is considered and the reflection, transmission and absorption coefficients are calculated based on this mode. The same can also easily be obtained for Transverse Electric mode as well.

3.3.1 Coefficient Derivation

The incident electromagnetic wave gives rise to a reflected wave in medium 1 and a transmitted wave in the medium 2 as shown in Figure 3.1. Thus the magnetic field in medium 1 can be written as a superposition of an incident wave and a reflected wave as below:-

a) $\mathbf{H}_1(\mathbf{r}) = \mathrm{H}_1(\mathrm{x,z})\hat{\mathbf{y}} = (\mathrm{H}_i e^{i\gamma_1 z} + \mathrm{H}_r e^{-i\gamma_1 z})\mathrm{e}^{i(\beta x - \omega t)}.\hat{\mathbf{y}}$,

while the transmitted wave can be written as

b) $\mathbf{H}_2(\mathbf{r}) = \mathrm{H}_2(\mathrm{x,z})\hat{\mathbf{y}} = \mathrm{H}_t e^{i\gamma_2 z}\mathrm{e}^{i(\beta x - \omega t)}.\hat{\mathbf{y}}$

where, $\beta^2 + \gamma_j^2 = \omega^2\mu_j^2\epsilon_j^2$ and,

γ_j denotes the z component of the wave vector in medium 1 and 2 for j=1 and 2, while β denotes the x component of the wave vector and ω defines the frequency of the wave. The relationship between β and ω is known as the dispersion relation which is determined by the property of the medium the wave is propagating through. From the dispersion relation one obtains the bandstructure of a material as discussed in chapter 1.

Now using the third Maxwell's equation, the Electric fields in each medium can be obtained as follows:-

a) $\mathbf{E}_1(\mathbf{r}) = \mathbf{E}_1(\mathrm{x,z}) = -\frac{1}{\omega\epsilon_1}(\hat{\mathbf{z}}\beta\mathbf{H}_1(\mathrm{x,z}) - \hat{\mathbf{x}}\gamma_1(H_i e^{i\gamma_1 z} - H_r e^{-i\gamma_1 z})\mathrm{e}^{i(\beta x - \omega t)})$

and

b) $\mathbf{E}_2(\mathrm{x,z}) = -\frac{1}{\omega\epsilon_1}(\hat{\mathbf{z}}\beta - \hat{\mathbf{x}}\gamma_2)\mathbf{H}_2(\mathrm{x,z})$

In order to proceed further, one now needs to apply the two boundary conditions, which states that the tangential component of the electric field is continuous across the

interface while the tangential component of the magnetic field is discontinuous across the same interface. Mathematically it can be written as below

$$\hat{z} \times (\mathbf{E}_2 - \mathbf{E}_1) = 0 \tag{3.5}$$

$$\hat{z} \times (\mathbf{H}_2 - \mathbf{H}_1) = -\sigma \hat{\mathbf{x}}\mathbf{E} \tag{3.6}$$

Using the above boundary conditions one obtains

$$E_1(x,0) = E_2(x,0)$$
$$H_2 - H_1 = -\sigma E_2(x,0)$$

Now applying the above two equations for the two mediums one obtains,

$$\frac{\gamma_1}{\epsilon_1}(H_i - H_r) = \frac{\gamma_2}{\epsilon_2}H_t$$
$$(H_i - H_r) = \frac{\gamma_2\epsilon_1}{\gamma_1\epsilon_2}H_t$$
$$H_t - H_r - H_i = -\sigma\frac{\gamma_2}{\omega\epsilon_2}H_t$$

Dividing both the sides with H_i, one obtains the transmission coefficient as

$$t = \frac{H_t}{H_i} = \frac{2\gamma_1\epsilon_2}{\gamma_1\epsilon_2 + \gamma_2\epsilon_1 + \sigma\gamma_1\gamma_2/\omega} \tag{3.7}$$

In the similar fashion, the reflection coefficient, r can also be obtained as

$$r = \frac{H_r}{H_i} = \frac{\gamma_1\epsilon_2 - \gamma_2\epsilon_1 + \sigma\gamma_1\gamma_2/\omega}{\gamma_1\epsilon_2 + \gamma_2\epsilon_1 + \sigma\gamma_1\gamma_2/\omega} \tag{3.8}$$

The absorption coefficient is given as $A = 1 - |r|^2 - |t|^2$.

3.3.2 Numerical

Now for some angles of incidence, and considering both intra band and interband transitions for the conductivity, σ as discussed in the previous chapter the graphs for absorption, reflection and transmission are shown in Figures 2,3 and 4 respectively.
These graphs shows the comparison of the analytical results obtained as above for various angles of incidence and that from the numerical results, obtained by COMSOL. It

shows a very good overlap between these results with divergence of only ± 0.01%. In COMSOL the RF module is used to solve this problem.

It shows that the transmission decreases as the angle of incidence increases which is quite understandable as the dielectric layer acts as a reflector in this case. And as expected the absorbance also decreases at first and then becomes a constant in the visible frequency range around 0.15% due to presence of impurities from the SiO_2 substrate. It has been shown in earlier experiments that the absorbance becomes constant to 2.3% for a free standing graphene that is when both the mediums are air. Analytically, also it can be easily shown.

3.3.3 Absorption for a suspended graphene layer

Considering a normal incidence, the amplitude of the transmission and reflection coefficient can be simplified to

$$R = -\frac{\sigma\omega\mu_0}{2\gamma_0 + \sigma\omega\mu_0} and \tag{3.9}$$

$$T = \frac{2\gamma_0}{2\gamma_0 + \sigma\omega\mu_0} \tag{3.10}$$

where, $T = |t|^2$ and $R = |r|^2$

Now applying these coefficients in $A = 1 - |r|^2 - |t|^2$, one obtains,

$$A = \frac{\eta_0 Re(\sigma)}{|1 + \sigma\omega\mu_0|^2} \tag{3.11}$$

where η_0 is the vacuum impedance which is approximately 377. At the high frequencies as discussed in the previous chapter, the graphene conductivity takes the value $e^2/4\hbar$ since interband transitions dominate and therefore the term A $\approx \eta_0 \frac{e^2}{4\hbar} = .02267 \approx 2.3\%$.

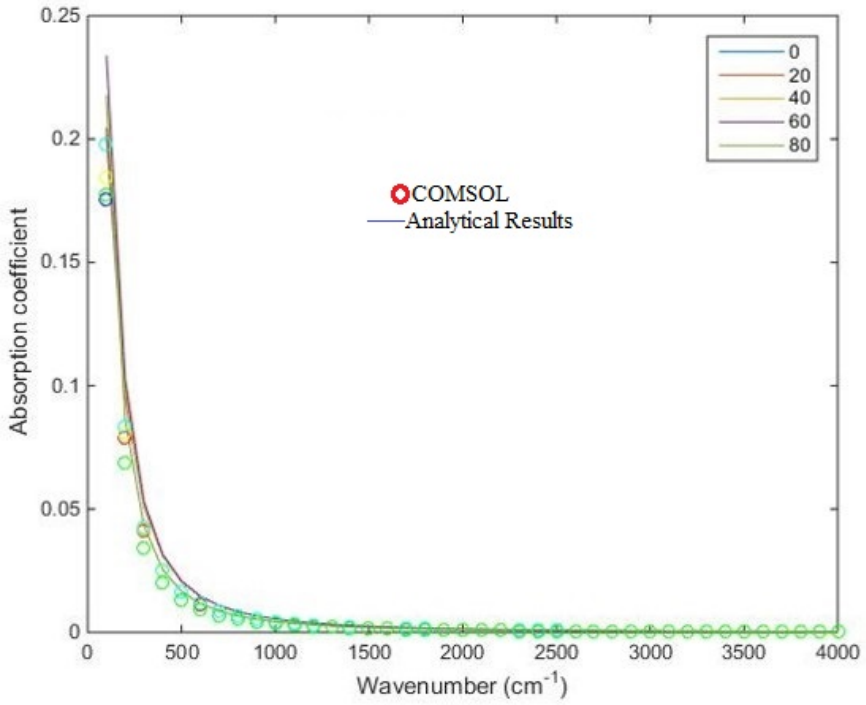

Figure 3.2: Absorption Plot

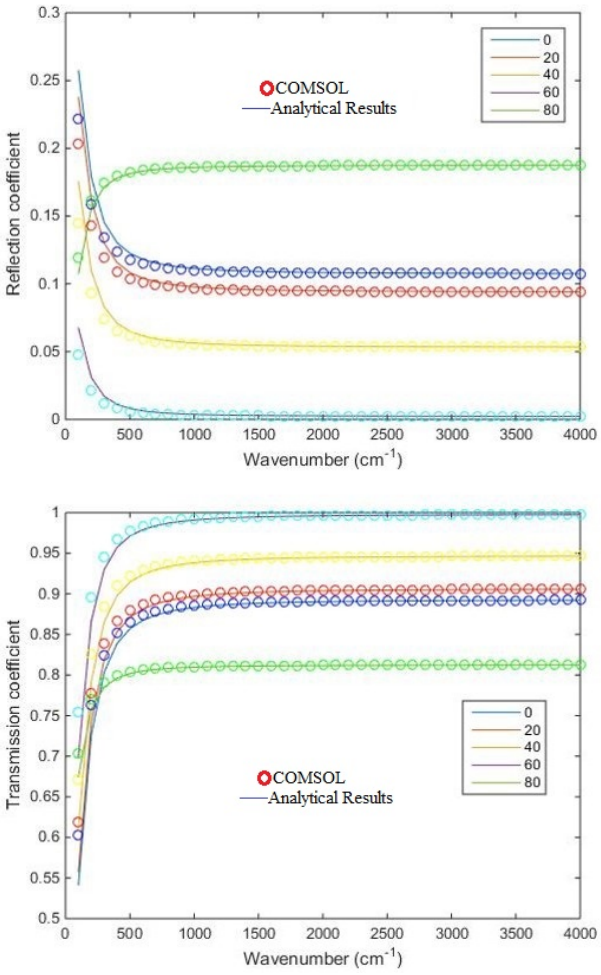

Figure 3.3: (a) Reflection plot comparison for various incident angles (b) Transmission comparison for various incident angles

Chapter 4

Graphene Nanoribbons: A study of the Electromagnetic Modes

4.1 Basic Idea of Nanoribbons

Graphene was first formed into nanometer width strips by the scientists of Swiss Federal Laboratories for Materials Science and Technology, Switzerland in 2010 where they used the bottom up fabrication technique [24]. The main aim behind the development of this nanoribbon structure was to use graphene in the channels of the field effect transistors. Therefore, this design attracted quite a good amount of attention, especially due to its stability at high temperatures (around 450 degree Celsius), which is the working environment of the current CMOS. Although many theoretical designs and electron transport calculations of these structures have been done since 2000 [15], but the experimental realization finally paved the way for better and advanced technological advancements.

This chapter is organized in the following fashion. In the first section, the basic simulational and analytical studies are going to be discussed for a nanoscale graphene strip, followed by graphene nanoribbons for various widths and then in the subsequent section, a comprehensive study is given on the surface plasmon modes that are formed in these

Nano-structures.

4.2 Basic Simulations and Analytical Calculations

The first calculations that were done was calculating the electromagnetic properties of a graphene nanometer on a dielectric substrate(we used SiO2) and observe the optical properties. As can be seen (the geometry: from the inset of Fig 1) the graphene strip (the blue line shown at the center) is 300nm in width is sandwiched between air and the SiO2 substrate. When electromagnetic wave (in THz to far IR range) is incident from the top, the electromagnetic response that was observed due to the electron oscillations is also shown in Figure 1. Both the analytical and simulation comparisons have been done and the analytic calculations are attached at the end of the chapter.

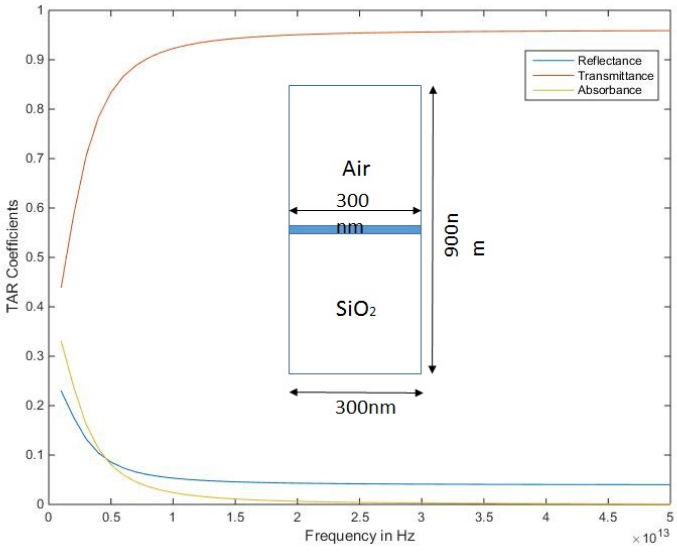

Figure 4.1: Transmission, Reflection and Absorption coefficient of a graphene sheet on SiO2

This study is performed with the Drude Model of conductivity. Although the Drude Model as shown in the previous chapter fails in the higher frequency range where inter-band transitions prevails in graphene, still, we are using this model since all these studies are limited from THz to far IR regime where the Drude conductivity works perfectly.

Another reason to use this model was to check the validity of the analytical results with the simulation studies and this model has a simpler mathematical approach. The thickness of the graphene layer is assumed to be 1nm and the relaxation energy to be 10meV which gives a relaxation time of 0.6 picosecond. The chemical potential is taken as 0.5eV and the calculations are done from 0 to 50 THz due for the better tunability of graphene in this spectrum [16]. The studies are done with the polarization of the incident field perpendicular to the width of the ribbon. From the obtained results, it is seen that the transmission is very high which means that the absorption or the loss is low. It can be attributed to the fact that at this low energy regime(<2Ef) which is even less than the thermal energy, the small absorption is due to the intraband transitions of the free carriers only. All calculations are done at room temperature of 300 Kelvin.

4.3 Studies on Graphene Nanoribbons

In this section, the electromagnetic phenomenon for ribbons of various widths is studied as shown in the geometry and the corresponding electromagnetic response is shown in Figure 4.2.

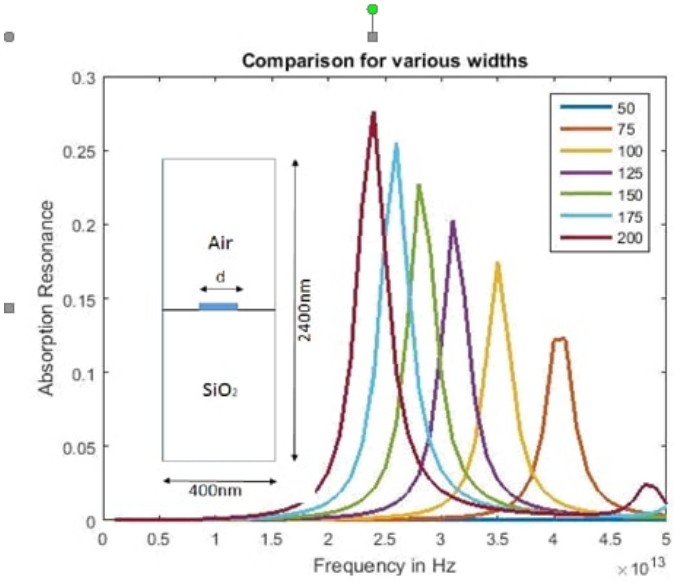

Figure 4.2: Graphene Nanoribbons Geometry and the corresponding Absorption Spectra

The various widths studied here are from 50 nanometers to 200 nanometers. Again, the same Drude model is used with the same polarization and other specifications as stated above. Prominent absorption peaks can be observed here which proves the presence of strong photon electron interactions (or, better known as light matter interaction) in this studied frequency region. It means that the collective oscillation strength of the electrons, which is termed as the plasma oscillations, is strong here. The two important advantages of using graphene nanoribbons here are 1) the light matter coupling of the incident EM wave is possible only in these engineered subwavelength nano structures. It cannot for example, couple with the electrons of the graphene sheets. And 2) these absorption peaks can also be obtained from a 2D-electron gas[2DEG] [17] at 4.2 Kelvin, but with graphene nanoribbons these peaks are observed even at room temperatures 300K. Moreover, the magnitude of these peaks is also greater than the 2DEG. It can be also be noticed from Figure4.2, how the resonance frequency gets tuned with the width of the nanoribbons. The resonance point shifts to higher energy when the width decreases, because, as the width gets smaller, the light confinement increases and thus strong plasmon oscillations prevails. The plasmon excitations varies with the width as $w^{-1/2}$. This scaling pattern have been shown to exist in 2DEG [18] and is followed in graphene nanoribbons as well.

Then the simple dispersion relations of the surface plasmons of these structures is studied and a discussion is done about the electromagnetic modes associated with it.

4.4 Surface Plasmon Modes in Graphene Nanoribbons

Surface plasmons(SP) are Transverse Magnetic (TM) mode electromagnetic waves, present along the interface between two mediums of different permittivity, which decays exponentially as it propagates. The solution of the Maxwells equation at a metal/dielectric interface gives the dispersion relation of the Surface Plasmon Polaritons (SPP) as follows (derived in the attached calculations): -

$$q_{sp} = \frac{\omega}{c}\sqrt{\frac{\epsilon_r \epsilon(\omega)}{\epsilon_r + \epsilon(\omega)}} \tag{4.1}$$

By solving the Maxwells equations for TM mode for our case shown above as in Figure4.1 (a graphene layer sandwiched between air (of relative permittivity, $\epsilon_r = 1$) and a dielectric substrate like SiO_2(whose relative permittivity $\epsilon_r = 1.5$)), considering graphene to have a conductivity of σ, the following surface plasmon dispersion relation (derived in the attached calculations) in the non retarded regime as (the calculations shown in supplemental pages)[meaning at small separation between the oscillating particles, $q >> \omega/c$) :-

$$q \ \frac{i2\omega\epsilon_r\epsilon_0}{\sigma(q,\omega)} \tag{4.2}$$

Now substituting model of conductivity in the above equation, the dispersion relation becomes,

$$q(\omega) \ \frac{2\pi\hbar^2\epsilon_0\epsilon_r}{e^2E_f}\omega^2(1 + i/\tau\omega) \tag{4.3}$$

By considering maximum light confinement, the plasmon dispersion can be calculated by setting the relaxation time to 0 as,

$$\omega_{pl} = \sqrt{\frac{e^2E_fq}{2\pi\hbar^2\epsilon_0\epsilon_r}} \tag{4.4}$$

To have a sanity check of this equation, the simulation results from COMSOL for different widths and the analytical model as described above are compared. It is assumed that the plasmonic resonances occur in a ribbon of width W when the wavevector, q is nearly equals to (2n+1) π/W [19] for n=0,1,2,3 and also when the unit cell lattice constant is twice the width of the ribbons [20]. The first condition means that the nanoribbon width permits half wavelength plasmon oscillations and thus the plasmonic modes with odd multiples can be present [21]. The figure 4.3 plot show the comparison of the same plasmon resonance data as in Fig 4.2 as a function of wave vector, q and compared it with the analytical model equation 4.4 for the same range of q.

The result shows a good overlap and thus a good verification of equation 4.2 in the non-retarded regime. The imaginary part of the wave vector, q(w), gives the propagation length of the surface plasmons. [Why is that? If we write the electric field, $E \approx Aexp(ikz - iwt)$ and express k as $k = k' + ik''$ and put it back in the expression, we get $E \approx Aexp(-k''z)exp(ik'z - iwt)$ implying the imaginary part gets coupled in the amplitude term A and it describes an exponential decay.]

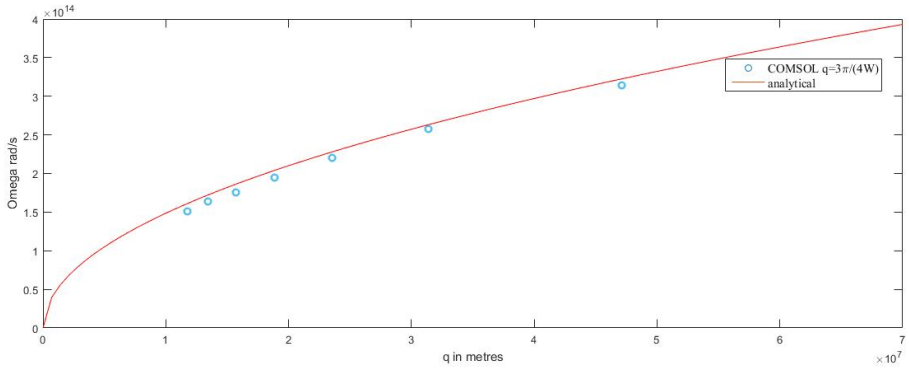

Figure 4.3: Comparison between the the Analytical and Simulational Model

4.4.1 Hybridized Surface Plasmon Modes in Graphene Nanoribbons

Localized surface plasmon resonance is observed when there is a collective oscillation of the conduction electrons. The localized field associated with this oscillation is evanescent in nature, but, when there is a collection of many particles, then the nature of this field changes, which leads to a change in the observed optical properties as well. The reason is that, when we have a collection of particles, there is also a mutual interaction of the fields among these particles, which leads to many possible effects. One of them is the splitting of the resonant frequency into two modes of differing energies. Hence, each plasmon resonance mode exists as a hybridization of an anti-symmetrically coupled plasmon mode of higher energy and a symmetrically coupled plasmon mode of lower energy. There are several models which explains this coupling or hybridization of the plasmons [22, 23]

The following two figures (Fig 4.4 and Fig 4.5) show the dispersion relation and the propagation length respectively, that we get by doing the eigen mode analysis of this nanoribbon structure in COMSOL. From the normalized dispersion plot, Figure 4.4, we see many modes have appeared. The first is the 2D graphene surface plasmon mode (2DGSP) (as shown with the red line) which can be related to an infinite graphene sheet, given by the relation, $q = \sqrt{(1 - 1/\alpha^2)}$ where $\alpha = 2/\pi\sigma c$ [derived while deriving equation 1] (attached in the Appendix). The second is the hybridized edge GSP (EGSP) mode which appears for a semi-infinite sheet of graphene.

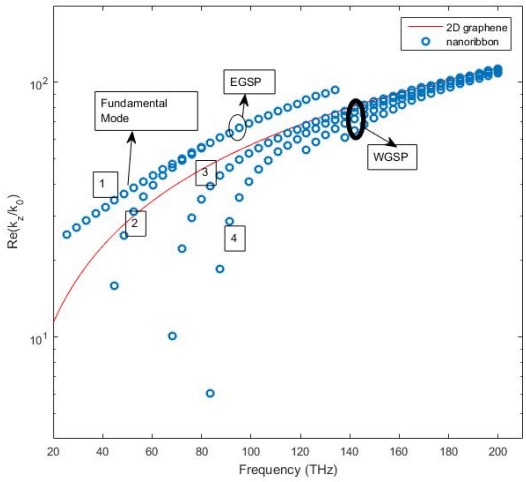

Figure 4.4: The Surface Plasmon Modes

From Figure 4.4, we can observe the two modes which have originated from the hybridization of the EGSP (marked as 1 and 2). The one with a greater magnitude of the normalized wave vector is termed as the fundamental mode. The second one originates at far infrared regimes, but converge into the fundamental EGSP mode of the semi-infinite sheet. We also notice that the magnitude of the fundamental mode is greater than the 2DGSP mode which means that the fundamental mode is more tightly confined than the 2DGSP.

The Figure 4.5 describes the propagation length of the modes, given by $2\pi/Imag(k)$. Due to tight confinement of the fundamental mode the propagation length is smaller than the 2DGSP, but at higher frequencies it merges with the 2DGSP. The reason of this behavior can be explained in terms of the conductivity in graphene. As seen in the last chapter on conductivity, we find that the conductivity decreases with the increase in frequency in the THz regime and then becomes a constant in the visible regime. Therefore from the relation,$\gamma = 2i\epsilon_0\omega/\sigma$ where γ is the Imaginary of (k), we see that γ, the wave vector component in the z direction increases with decrease in the conductivity. We know that the propagation length, L is given by $1/2/\gamma$. Hence with increase in γ we have a decrease in L and an increase in the confinement. For higher frequencies, when the conductivity becomes a constant, the γ is still large but coincides with the

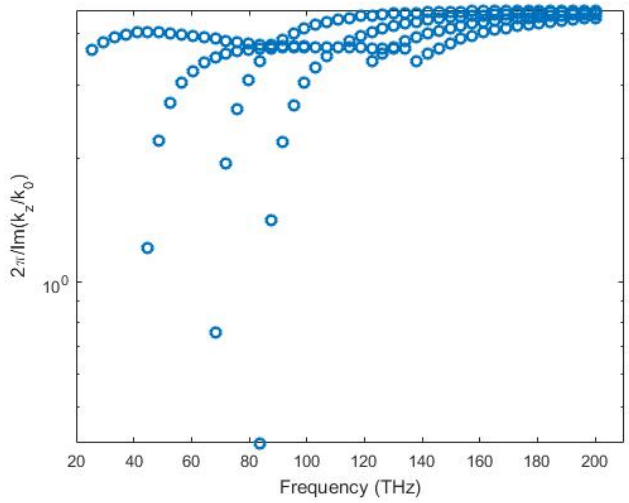

Figure 4.5: The Propagation Length of Surface Plasmon Modes

imaginary(q) of 2DGSP which means that the confinement is similar to that of EGSP. The third kind of modes that appears is the hybridized waveguide surface plasmon modes(WGSPs) (marked in Figure 4.4) as 3 and 4. They extend over the entire width of the ribbon , but their confinement is not as high as the 2DGSPs and hence they have a lesser confinement and higher propagation length.

Thus we have studied the electromagnetic properties in a graphene nanoribbon and compared our simulation results with the analytical model. Then we studied about the surface plamon dispersion characteristics in the THz range and found the existence of several types of modes, like the EGSPs which is concentrated across the edges, WGSPs which is found throughout the width and the 2DGSPs of an infinite graphene sheet.

Some of the disadvantages of using surface plasmons in graphene for waveguiding and other related applications are relative short lifetime and change in nanostructure geometry to control the plasmons while a great advantage is the large concentration of the EM waves bear the ribbon edges which can be useful to transfer information between neighboring waveguides.

Chapter 5

Metamaterials based on Split Ring Resonators and Gold

5.1 Introduction

The ability to manipulate the properties of the electromagnetic waves or light via specially designed geometrical structures is one of the most important development among the optics and material scientist fraternity for the past decade. This leads one to have an unprecedented control of the light-matter interaction and thus tune in the effective properties of the materials, thereby, allowing many of the theoretical concepts, like the negative refractive index [24] , cloaking [25] , perfect lenses [26] to be realized in real life. Metamaterials are made with artificially designed subwavelength structures that has the property to produce the desired electromagnetic response. This chapter, which is the main part of this thesis, describes the geometry and ways to control the optical properties of an array of structures. The geometry used here is the Split Ring Resonator(SRR) structures made from graphene. Results wih SRR made with gold is also shown. SRR are used to create magnetic response from materials which are non-magnetic otherwise. For example, graphene is purely a non-magnetic material. But using graphene in these split ring structures gives magnetic response although the magnitude is very small. All the simulation works are done with COMSOL.

5.1.1 Brief History of Metamaterials

The people from the early 1500s were probably the first to realize that light can be controlled is certain ways when they made stained glasses in the cathedrals to produce brilliant electromagnetic diffraction effects [27]. This shows that people of those era had already realized that the properties of naturally occurring materials are probably fixed and hence they need to make materials or structures to obtain the effects they want. The year 1968 probably marks the birth of the concept of metamaterial with the theoretical proposition made by Vaselago [28] of having a material medium with simultaneously occurring negative permittivity and negative permeability, which is termed as the Left Handed Media. However, this idea was not quite entertained by the scientific community at the time until 1996 when John Pendry and his group contributed two seminal propositions of preparing artificial structures with negative ϵ [29] and μ [30]. In 2000 the experimental realization of having such a medium with both $\epsilon < 0$ and $\mu < 0$ was shown by Smith and his group by using a periodic arrangement of complimentary split ring structures and wires in the microwave region. [31].

5.1.2 Meaning of negative index

According to Vaselago, waves propagating through this kind of media is known to have negative phase velocity and suffer negative refractive index. The consequence of having this kind of material with negative index is that the propagation direction ($\vec{k}$) of the EM wave through this medium is opposite to the propagation direction of the energy flow (the Poynting vector, S). For naturally occurring right handed materials which follow the general E,H,k right handed convention, the propagation direction is parallel to the Poynting vector. This means that in the LH media the propagation direction is reversed since the index is less than 0. The figure below shows this comparison:-

Since then tremendous research followed in this area with having Vaselago's paper cited for more than 10000 times. Initially research was more focused in the microwave region, but with advent of technologies, soon the visible to terahertz regime also became accessible. [32] But the actual realization was quite a challenge since it is hard to get a negative magnetic response from the materials. According to the parameters ϵ and μ, the metamaterials are classified as shown in the figure(5.2).

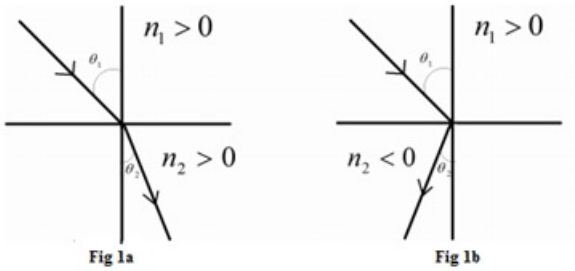

n.jpg

Figure 5.1: a)Right Handed Material b) Left Handed Materials

Although it has been later pointed out that one needs to have some kind of chirality present in the medium to see negative index [34]. This thesis is not based on negative index response since the magnetic response in graphene is very weak. Although, from gold, it is seen that there is a good magnetic response but it is not possible to have the negative index with just these split ring structure. Recently, Smith and his group have been able to demonstrate such effects using a composite structure of a rod and split ring [30]. The aim of this thesis is not negative index, but a study of the magneto-electric coupling in graphene or more specifically optical properties in non magnetic materials.

5.1.3 The basic physics of Metamaterials

The basic physics behind the optical phenomenon in metamaterials can be explained with reference to the atomic arrangements in naturally occurring materials. In normal materials the wavelength of the incident radiation is much larger than the atomic spacing in a lattice. Hence the characteristic length of the unit cell determines how the material will behave to the incident radiation. In simple terms, the transmission, absorption and reflection coefficients (TAR coefficients) will depend on the lattice structure of the material. This is a very basic problem in quantum mechanics and solid state physics of how the periodic/aperiodic arrangement of atoms affects the TAR coefficients and can be readily solved using the Schrodinger equation. What happens in metamaterial is that this periodic lattice structure is controlled and determines what the characteristic length of a unit cell be and thus have a control over the TAR coefficients. For example, in the previous chapter, studies are done on periodic arrangement of nanoribbon arrays. It is shown there how the width of the ribbons have a direct effect on the position of the

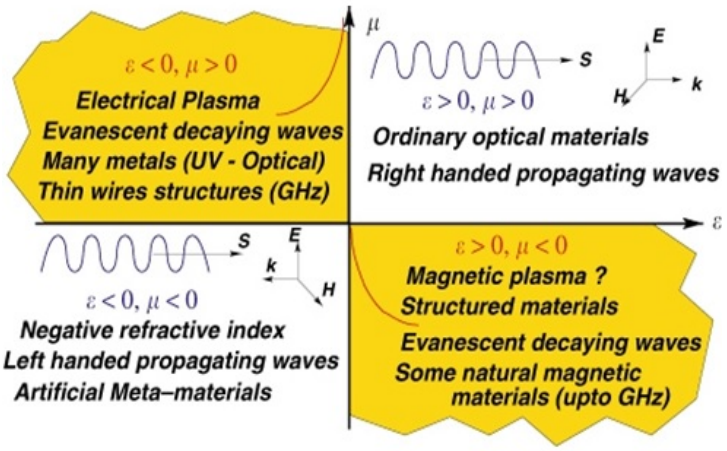

Figure 5.2: Metamaterials classification. Figure taken from [33]

resonance point. [The Figure 4.2 in the previous chapter can be considered as a unit cell of characteristic length of 400 nanometers]. Thus careful consideration is made while designing a metamaterial since this opens up a wide variety in the effective properties determination of this total periodic arrangement. This leads to one of the main aim of this thesis: homogenizing a periodic array of nanostructures such that the material behaves as a continuous medium in the long wavelength limit. This thesis studies the electromagnetic properties obtained from a periodic arrangement of split ring resonating structures in the nanoscale regime.

This chapter is designed in the following way. In the first part, the general absorption spectrum response for various geometrical arrangements of the split ring resonator structures will be discussed. Then the bianisotropy effect will be discussed in these structures followed by the development of the field equations inside the materials. The second part of the chapter will deal with homogenization of these periodic arrangements and methods to retrieve the effective parameters like, ϵ and μ, from the homogenized structure and the critical problem faced while incorporating analytical results with COMSOL. For a sanity check, a general dielectric lossy slab with known parameters is used and

the retrieval technique is applied there to do a consistency check and it can be seen that one gets back the same parameters that one starts with. The third part will deal with specific examples like the studies made with graphene and gold.

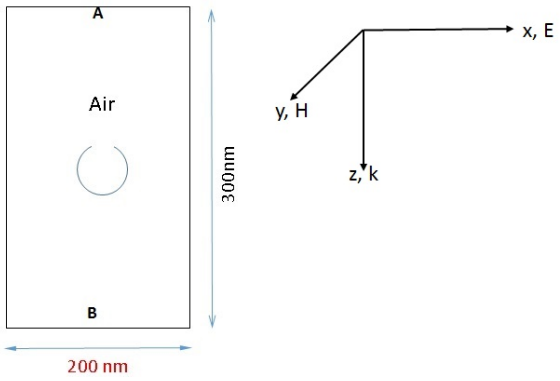

Figure 5.3: SRR Geometry and the wave configuration

5.2 The Split Ring Resonators: The Electromagnetic Response

The basic electromagnetic response studies are done with graphene split ring resonator structures with the geometry of a single unit cell as show in the figure 5.3. For the simplest possible case, it is considered that the graphene structure is suspended in an air medium with the exciting ports about 100nm away from the structure. The wave is propagating along the z-direction with the H-field coming out of the plane and the E-field along the plane of the split ring structure, shown in the same figure5.3 The same kind of parameters as done with graphene nanoribbons are used here as well. The first thing to mention is that the Kubo model of conductivity is again considered here because the range of frequency considered here goes nearly to the near infrared regimes. The damping energy is taken to be 10meV with a relaxation time approximation of 0.6 picoseconds and the doping is taken as 0.5eV. Three kinds of studies are done:-

i) By varying the gap width of the resonators keeping the radius constant, or in other words by varying the sector angles

ii) By varying the radius keeping the sector angle same and

iii) By varying the angle of incidence The absorption spectrum is very less, because mostly transmission is there. But the other most striking feature about these results is that the electromagnetic(EM) resonance spectrum is not the same when the excitation ports are different. It is found that the transmission is same from both the ports but the reflectance is different. The response shown below are for the three possible cases described above along with the relative difference in absorption spectrum when the ports are different.

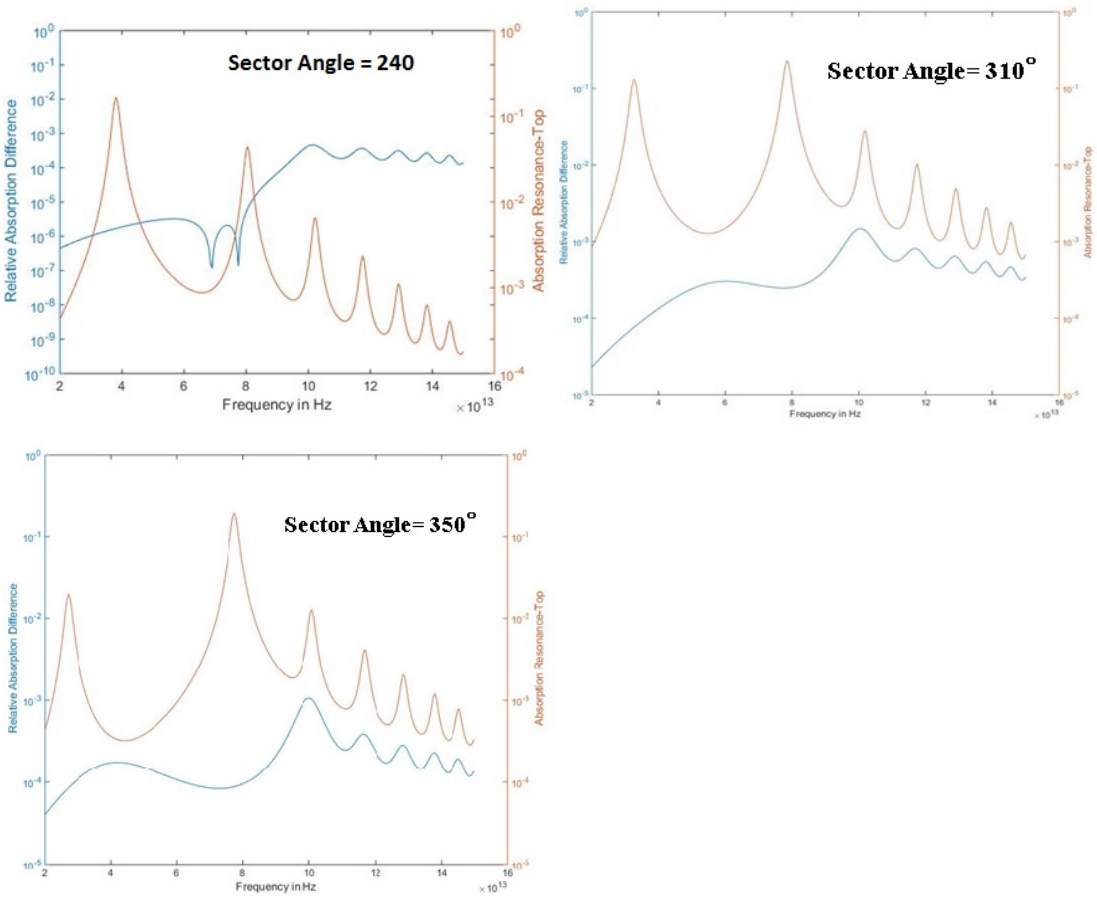

Figure 5.4: Response by varying the width of the gap same as controlling the sector angle: The blue line shows the relative absorption difference when light is incident from the top port and from the bottom port.

The blue line shows the relative absorption difference based on the following calculation:

-

$$RelativeAbsorptionDifference = \frac{Absorption_{top} - Absorption_{bottom}}{Absorption_{top} + Absorption_{bottom}} \tag{5.1}$$

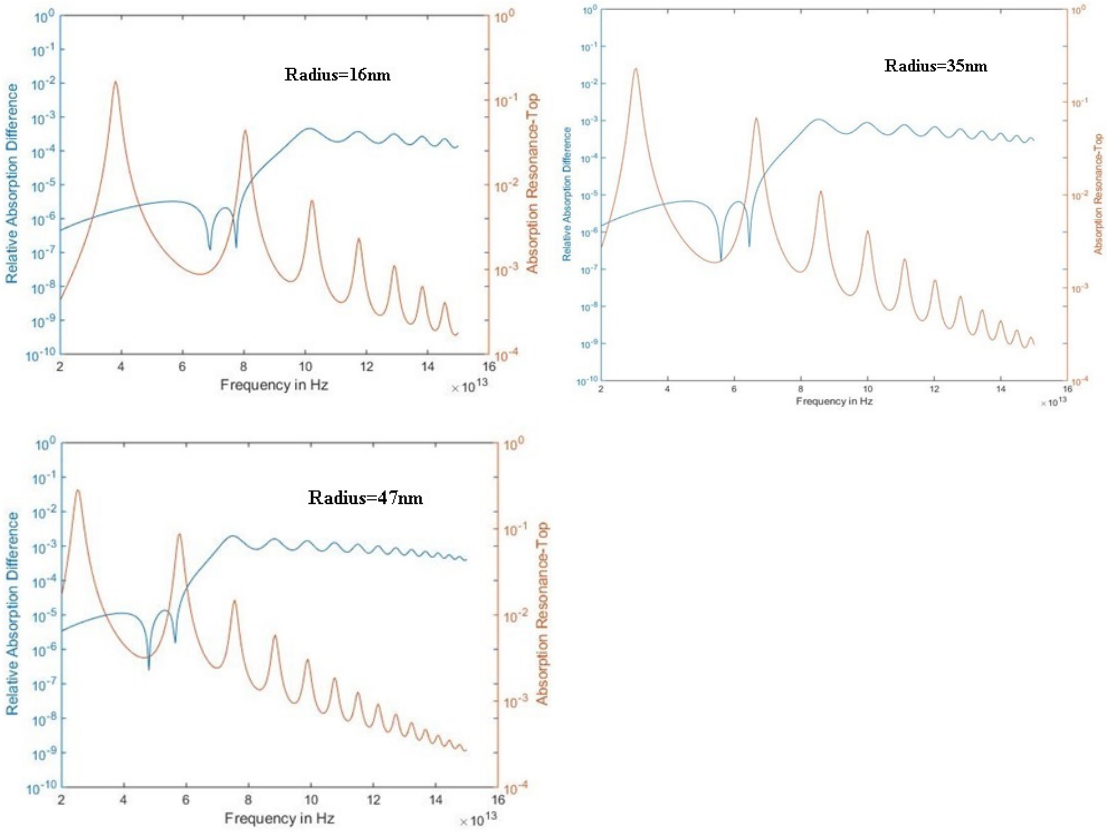

Figure 5.5: Response by varying the radius of the sector: The blue line shows the relative absorption difference when light is incident from the top port and from the bottom port.

Many cases are particularly studied in order to understand whether this phenomenon is due to any numerical errors or is relevant for all possible cases. Although another important point to state here is that all these studies are done with the TM mode polarization of the incident wave. When the TE mode polarization is used for this specific geometry, shown in Fig5.3 then no such effects are observed. This led to more literature surveys [38, 39] and finally the development of the concept of bianisotropy. Bianisotropy can be defined in two ways. When there is lack of inversion symmetry

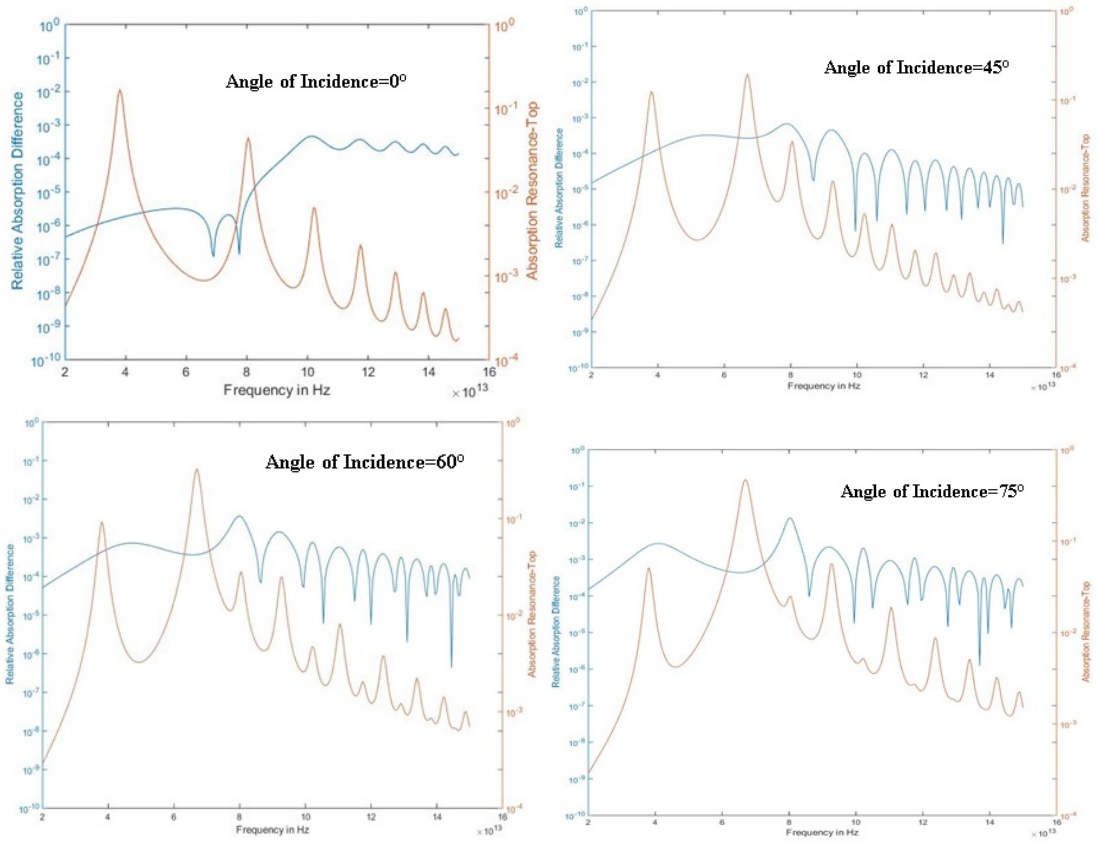

Figure 5.6: Response by varying the angle of incidence: The blue line shows the relative absorption difference when light is incident from the top port and from the bottom port.

along the propagation direction, k of an EM wave, then this kind of difference in absorption and reflectance spectrum is observed when the opposite ports are excited. This phenomenon is defined as bianisotropy as has been described in many literatures [39]. If the k is in the x direction rather than in the z-direction, then there will be absence of bianisotropy because the structure will then be symmetric to the propagation direction, k. Now transmission is equal in magnitude both the sides because transmission does not depend on the geometry of the structure. The second definition of bianisotropy will be given while deriving the EM polarization response of these split ring structures. And then it can also be seen why these bianisotopy effects is present for a specific case of polarization only.

5.2.1 Deriving the field equation inside

The incident electromagnetic field convention is shown in the figure below. As mentioned the TM mode is used with H along the y direction(coming out of the plane) and the E-field along x while the wave is propagating along the z direction.

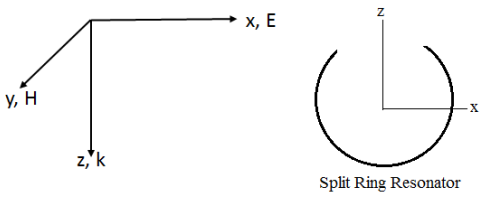

Figure 5.7: The geometry of the SRR structure and the E,H,k convention

The SRR can be modeled as a series circuit comprising of an inductor formed via the closed loop wire and a capacitor formed by the two ends of the wire, thus forming a series LC circuit with a resonance frequency of $\omega = \sqrt{1/LC}$. The incident E field of the electromagnetic radiation is along the gap of the SRR, which produces a circulating oscillatory current, giving rise to a magnetic field perpendicular to the plane of the SRR. Similarly the time varying H-field of the incident radiation will also give rise to a circulatory current along the wire. Thus both the E and H fields of the incident radiation are responsible for simultaneous excitation of electric and magnetic dipoles.

The mathematical model can be derived by assuming harmonically varying incident electric and magnetic fields,
$E_x(t) = E_x \exp(i\omega t)$+c.c and $H_y(t) = H_y \exp(i\omega t)$+c.c.
Two cases for current production are considered, first the current produced when there is a change in the magnetic flux and second the current produced when there is a change in the electric flux.
In general, the voltage induced in the split ring structure can be given as,

$$U_{ind} = \frac{1}{C}\int Idt + IR + L\frac{dI}{dt} \tag{5.2}$$

This voltage induced can be due to two reasons- one due to changing magnetic flux and second due to changing E-field. Each cases are considered separately.
Considering current induced by the changing magnetic flux, we get,
$U_{ind} = -\frac{\partial \phi}{\partial t}$ where, $\phi(t) = \mu_0 H_y(t) l^2$

Taking a sinusoidal variation of $I(t) = I\exp(i\omega t)$+cc, we get

$$U_{ind} = \frac{1}{C}\frac{I(t)}{i\omega} + I(t)R + i\omega L I(t)$$
$$i\omega\mu_0 H_y(t) l^2 = I(t)[\frac{1}{i\omega C} + R + i\omega L]$$
$$I = \frac{\omega^2 \mu_0 l^2 H_y(t) C}{1 + i\omega RC - \omega^2 LC}$$

$$\boxed{I = \frac{\omega^2 h H_y}{\omega_{LC}^2 - \omega^2 + i\gamma\omega}} \tag{5.3}$$

where, $\gamma = \frac{R}{L}, L = \frac{\mu_0 l^2}{h}, \omega_{LC}^2 = \frac{1}{LC}$
This current as shown below is responsible for both the magnetic polarization and electric polarization which can be found as follows:-

Magnetic Dipole Density

$$M_y(t) = \frac{1}{a_{xy}^2 a_z} I(t) l^2$$
$$M_y(t) = \frac{1}{a_{xy}^2 a_z}\frac{\omega^2 h H_y l^2}{\omega_{LC}^2 - \omega^2 + i\gamma\omega}$$

$$\boxed{M_y(t) = \frac{\omega^2 F}{\omega_{LC}^2 - \omega^2 + i\gamma\omega} H_y} \tag{5.4}$$

where, F is split ring volume filling fraction given by, $\frac{l^2 h}{a_{xy}^2 a_z}$

Electric Polarization

$$P_x(t) = \frac{1}{a_{xy}^2 a_z} \int I dt$$

$$P_x(t) = \frac{dI}{a_{xy}^2 a_z i\omega} P_x(t) = \frac{d}{a_{xy}^2 a_z i\omega} [\frac{\omega^2 l^2 \mu_0 C H_y}{1 + i\omega RC - \omega^2 LC}]$$

$$P_x(t) = \frac{d\omega l^2 \mu_0 H_y}{i a_{xy}^2 a_z} \frac{1}{LC} [\frac{1}{\frac{1}{LC} + i\omega\frac{R}{L} - \omega^2}]$$

$$P_x(t) = \frac{F d\omega}{i l^2} \frac{1}{\omega_{LC}^2 + i\gamma\omega - \omega^2} H_y$$

$$\boxed{P_x(t) = -\frac{i d F \omega}{l^2(\omega_L^2 + i\gamma\omega - \omega^2)} H_y} \tag{5.5}$$

This means there is both electric and magnetic polarizations due to the magnetic field of the incident wave.

Next considering the current induced by the electric field, we get,
$U_{ind} = E_x(t)d$

$\implies E_x(t)d = \frac{1}{C} \int I dt + IR + L\frac{dI}{dt}$

$\implies E_x(t)d = I[\frac{1}{i\omega C} + R + i\omega L]$

$\implies I = \frac{i\omega C E_x d}{LC[\frac{1}{LC} + i\omega\frac{R}{L} - \omega^2]}$

$$\implies \boxed{I = \frac{i\omega E_x d}{L[\omega_{LC}^2 + i\gamma\omega - \omega^2]}} \tag{5.6}$$

where, $\gamma = R/L$ and $\omega_{LC} = \sqrt{LC}$
Similarly as before we can find the magnetic polarization using,

$M_y(t) = \frac{1}{a_{xy}^2 a_z} I(t) l^2 E_x$

Substituting $L = \frac{\mu_0\ l^2}{h}$ and $F = \frac{l^2 h}{a_{xy}^2 a_z}$ and $\gamma = R/L$,

we get,

$$\boxed{M_y(t) = \frac{1}{\mu_0}\frac{d}{l^2}\frac{i\omega E_x F}{\omega_{LC}^2 + i\gamma\omega - \omega^2}} \tag{5.7}$$

Similarly, the electric polarization induced is given by,

$$\boxed{P_x(t) = \frac{1}{\mu_0}(\frac{d}{l^2})^2\frac{F}{\omega_{LC}^2 + i\gamma\omega - \omega^2}E_x} \tag{5.8}$$

Now using $D_x = \epsilon_0 E_x + P_x$ and $B_y = \mu_0(H_y + M_y)$

$$\begin{bmatrix} D_x \\ B_y \end{bmatrix} = \begin{bmatrix} \epsilon_0\epsilon & ic_0^{-1}\xi \\ -ic_0^{-1}\xi & \mu\mu_0 \end{bmatrix} \times \begin{bmatrix} E_x \\ H_y \end{bmatrix} \tag{5.9}$$

with

$M_y = \frac{\omega^2 F}{\omega_{LC}^2 - \omega^2 + i\gamma\omega} H_y$

$P_x = -\frac{idF\omega}{l^2(\omega_L^2 + i\gamma\omega - \omega^2)} H_y$

$M_y = \frac{1}{\mu_0}\frac{d}{l^2}\frac{i\omega E_x F}{\omega_{LC}^2 + i\gamma\omega - \omega^2} E_x$

$P_x = \frac{1}{\mu_0}(\frac{d}{l^2})^2 \frac{F}{\omega_{LC}^2 + i\gamma\omega - \omega^2} E_x$

The term ξ is the bianisotropic or the magnetoelectric coupling factor. Now when the material is anisotropic in nature in all the three x,y and z plane, all these parameters that is the ϵ, μ and xi then each becomes a 3×3 tensor and the matrix of equation5.2.1 becomes a 6× matrix. In this thesis, since a single layer of 2D graphene is used which is rolled to make a cylindrical structure, and moreover the Hamiltonian in graphene is considered to be near the symmetry points, the graphene is considered to be isotropic in nature and hence the off-diagonal elements of the parameters are taken to be zero while the diagonal elements are equal. The equations derived here are used while deriving the equations for the parameter retrieval.

5.2.2 Parameter Retrieval from the S-parameters

The geometry shows a periodic arrangement of the single SRR unit cell structure. The unit cell as marked in blue is considered to be a square of 200nm.

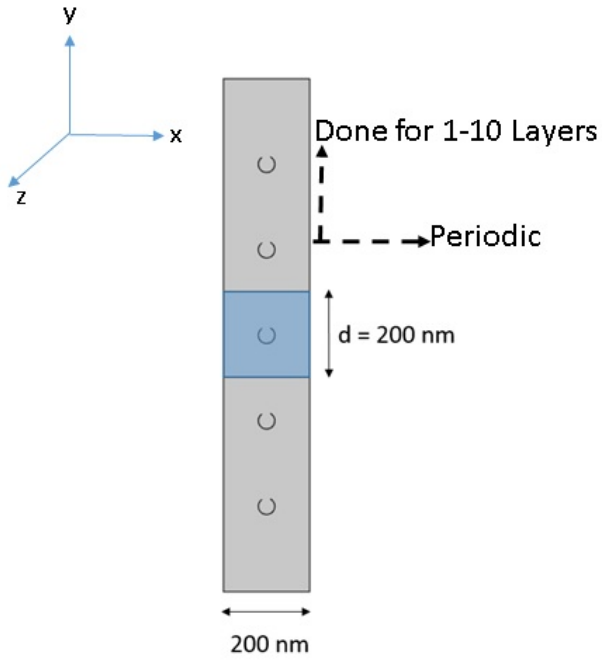

Figure 5.8: The geometry of the SRR structure and the E,H,k convention

As mentioned before the aim of the thesis is to homogenize this periodic arrangement so that it can be used as a continuous material in the long wavelength limit. This continuous material present bulk properties when the characteristic length of each unit cells is several times smaller than the wavelength of light. Hence the determination of these effective electromagnetic parameters becomes a necessity to have an understanding of the metamaterial behavior without having any knowledge of the local field distribution inside the structure. There are many existing methods to calculate such effective parameters [40, 41, 42], but most of these methods are restricted to anisotropic or isotropic structures. Since a SRR is bianisotropic in nature, so these methods cannot be applied for these structures. The method used for this thesis is pretty straight forward and can be applied to any materials. This method is closely aligned with that followed in

[43]. Owing to reciprocity, as mentioned before the transmittance does not depend on from which the light is impinging on the metamaterial, but due to lack of symmetry reflectance does depend. So there are only three complex S-parameter terms (−the two reflectance terms(r_+ and r_-) and one transmittance term), obtained from COMSOL- the two reflectance terms obtained from the two sides of the port and one transmittance term. These complex electromagnetic terms depend on the parameters ϵ, μ and ξ(the bianisotropy term). The retrieval method used here is done by using simple Maxwells equations to invert these complex field terms and derive ϵ, μ and ξ in terms of complex fields. The first part shows the formulation of Maxwells equations in a material and the second section shows the parameter retrieval.

5.2.3 Maxwell's equation in the metamaterial slab

Taking the following conventions of the Electric field and Magnetic fields,
$E^{\pm} = E^{\pm}\exp(i\omega t \mp kz)\hat{x}$ and
$H^{\pm} = H^{\pm}\exp(i\omega t \mp kz)\hat{y}$,
where $\pm$ denotes the propagation in the negative z direction and positive z direction respectively. The reason to choose $\exp(+\mathrm{i}\omega t)$ sign convention is because the the reflectance, transmittance parameters are derived from COMSOL and this finite element software follows $+i\omega t$ sign convention.
First considering the motion in the positive z direction, and using the Maxwell's equation,
$\vec{\bigtriangledown} \times E^+ = -\frac{dB_y}{dt}$
we get,
$\vec{\bigtriangledown} \times E^+ = -ikE^+\exp(-ikz)\exp(i\omega t)\hat{y}$ and by using equation
$\frac{dB_y^+}{dt} = [\frac{\omega}{c_0}\xi E^+ + i\omega\mu\mu_0 H_y^+]\exp(i\omega t)exp(-ikz)$
Now equating the two equations, we get,
$E^+[ik - \frac{\omega}{c_0}\xi] = i\omega\mu\mu_0 H^+$
Therefore, $\frac{E^+}{H^+} = \frac{i\omega\mu\mu_0}{ik - \frac{\omega}{c_0}\xi}$ which is also denoted by Z^+ and known an Bulk Impedance.
Now taking $k = n\frac{\omega}{c_0}$and $z_+ = Z_+/Z_0$ where $Z_0 = \sqrt{\frac{\epsilon_0}{\mu_0}}$ and expressing $c_0 = \frac{1}{\sqrt{\epsilon_0\mu_0}}$, we get,
$z_+ = \frac{i\mu}{in - \xi}$

$z_+ = \frac{\mu}{n+i\xi}$

Now using Maxwell's Equations when the wave is propagating in the reverse direction, that is,

$\vec{\bigtriangledown} \times E^- = -\frac{dB_y}{dt}$ we get,

$\vec{\bigtriangledown} \times E^- = ikE^- \exp(ikz)\exp(i\omega t)\hat{y}$ and

$\frac{dB_y^-}{dt} = [\frac{\omega}{c_0}\xi E^- + i\omega\mu\mu_0 H_y^-]\exp(i\omega t)exp(ikz)$

Now equating the two equations,

$E^-[ik + \frac{\omega}{c_0}\xi] = -i\omega\mu\mu_0 H^-$ Therefore, $\frac{E^-}{H^-} = -\frac{i\omega\mu\mu_0}{ik+\frac{\omega}{c_0}\xi}$ which is also denoted by Z^-.

Again taking $k = n\frac{\omega}{c_0}$and $z_- = Z_-/Z_0$ where $Z_0 = \sqrt{\frac{\epsilon_0}{\mu_0}}$ and expressing $c_0 = \frac{1}{\sqrt{\epsilon_0\mu_0}}$, we get,

$z_- = \frac{\mu}{-n+i\xi}$

Thus the two impedances are

$z_\pm = \mu(\pm n + i\xi)^{-1}$ Now the aim is to find these parameters in terms of the reflectance, transmission coefficients.

5.2.4 Parameter Retrieval: Using the Boundary conditions

Applying the boundary conditions at the homogenized two interfaces of the metamaterials, which are considered tobe at z = 0 and z = ds respectively, where ds is the effective length of the metammaterial, for the first interface it can be written as

$$\begin{aligned} E_i + E_r &= E_+ + E_- \\ 1 + \frac{E_r}{E_i} &= E_+ + E_- \\ (1 + r_+)E_i &= E_+ + E_- \end{aligned} \tag{5.10}$$

For H-fields, the reflection coefficient can also be computed as below:-

$$\begin{aligned} \frac{E_i}{z_1} + \frac{E_r}{-z_1} &= \frac{E_+}{z_+} + \frac{E_-}{z_-} \\ (1 - r_+)\frac{E_i}{z_1} &= \frac{E_+}{z_+} + \frac{E_-}{z_-} \end{aligned} \tag{5.11}$$

At the other boundary of the metamaterial, that is at z=ds, the boundary conditions can respectively be written for the E-field and H-field as

$$E_+ e^{-ink_0 ds} + E_- e^{ink_0 ds} = t_+ E_i \tag{5.12}$$

$$E_+ e^{-ink_0 ds}/z_+ + E_- e^{ink_0 ds}/z_- = t_+ E_i/z_2 \tag{5.13}$$

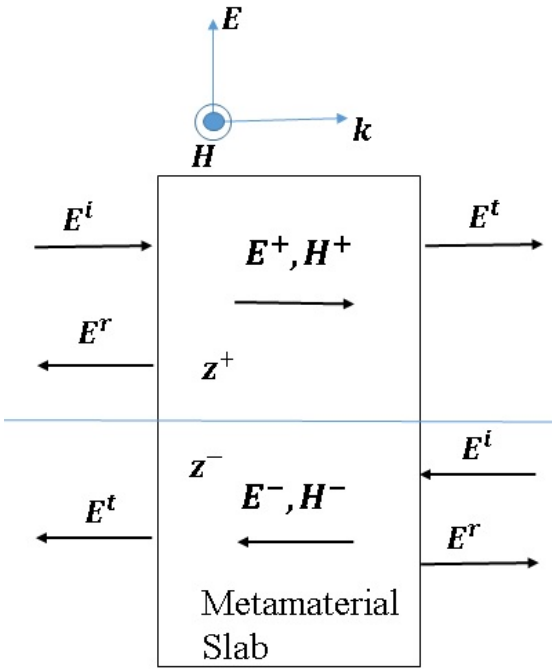

Figure 5.9: The homogenized material

The main aim now is to find n, z_+ and z_- in terms of r_+, r_-, t_+ and t_- from these equations by using basic algebra. Some of the primary steps are explained below. Using the equations 5.10 and 5.11, E_+ can be eliminated by simple algebra and E_-/E_i can be computed as

$$\frac{E_-}{E_i} = (1 - \frac{z_1}{z_+} - r_+(1 + \frac{z_1}{z_+}))\frac{z_+ z_-}{z_1(z_+ - z_-)} \tag{5.14}$$

Similarly from equations 5.12 and 5.13, E_-/E_i is

$$\frac{E_-}{E_i} = t_+ e^{ink_0 ds}\frac{z_-(z_+ - z_2)}{z_2(z_+ - z_-)} \tag{5.15}$$

The above equations 5.14 and 5.15 are both equal to E_-/E_i and they can be equated and t_+ is computed as

$$t_+ = e^{-ink_0 ds}(1 - \frac{z_+}{z_1})(1 - \frac{z_+}{z_2})^-1 + r_+ e^{-ink_0 ds}(1 + \frac{z_+}{z_1})(1 - \frac{z_+}{z_2})^-1$$

For simplicity it can be written as

$$\boxed{t_+ = \gamma + \delta r+} \tag{5.16}$$

where
$\delta = e^{ink_0ds}(1 + z_+/z_1)(1 - z_+/z_2)^{-1}$
$\gamma = e^{ink_0ds}(1 - z_+/z_1)(1 - z_+/z_2)^{-1}$
Similarly arranging the boundary conditions, the two equations of E_+/E_i can be computed as

$$\frac{E_+}{E_i} = t_+ e^{-ink_0ds} \frac{(z_2 - z_-)}{z_2 z_-)} \frac{z_+ z_-}{(z_+ - z_-)} \tag{5.17}$$

$$\frac{E_+}{E_i} = \frac{z_+ z_-}{z_1(z_+ - z_-)}((\frac{z_1}{z_-} - 1) + r_+(1 + \frac{z_1}{z_-})) \tag{5.18}$$

Therefore again combining equation 5.17 and 5.18 one gets,

$$t_+ e^{-ink_0ds}(1 - \frac{z_-}{z_1})(1 - \frac{z_-}{z_2})^-1 + r_+ e^{-ink_0ds}(1 + \frac{z_-}{z_1})(1 - \frac{z_-}{z_2})^-1 \tag{5.19}$$

Again a simplified version of the above equation can be written as

$$\boxed{t_+ = \alpha + \beta r_+} \tag{5.20}$$

where
$\alpha = e^{-ink_0ds}(1 - z_-/z_1)(1 - z_-/z_2)^{-1}$
$\beta = e^{-ink_0ds}(1 + z_-/z_1)(1 - z_-/z_2)^{-1}$

Now considering the propagation of the wave in the reverse direction the same aim is to find similar relations as above between t_- and r_-. When the wave propagates in the opposite direction we just need to take the following change in the sign conventions, $z_1 \Rightarrow -z_2$, $z_2 \Rightarrow -z_1$, $z_+ \Rightarrow z_-$ and $z_- \Rightarrow z_+$
Therefore the following relations are obtained:
$t_- = \alpha' + \beta' r_-$ and
$t_- = \gamma' + \delta' r_-$ where,
$\alpha' = e^{-ink_0ds}(1 + z_+/z_2)(1 + z_+/z_1)^{-1}$
$\beta' = e^{-ink_0ds}(1 - z_+/z_2)(1 + z_+/z_1)^{-1}$

$\delta' = e^{ink_0 ds}(1 - z_-/z_2)(1 + z_-/z_1)^{-1}$
$\gamma' = e^{ink_0 ds}(1 + z_-/z_2)(1 + z_-/z_1)^{-1}$

Now by doing some simple algebra of the above mentioned equations one can find a simple polynomial in z+ and z- as below:-
$z_-^2(t_+t_-(1-r_+)(1-r_-)) + z_-((z_1-z_2)(t_+t_-+1-r_+r_-)+(z_1+z_2)(r_+-r_-)) + z_1z_2((1+r_+)(1+r_-) - t_+t_-) = 0$

Hence z_- can be expressed as

$$z_- = \frac{-b + \sqrt{b^2 - 4ac}}{2a} \tag{5.21}$$

$$\textbf{and } z_+ = \frac{b - \sqrt{b^2 - 4ac}}{2a} \tag{5.22}$$

where,
$a = t_+t_- - (1 - r_+)(1 - r_-)$
$b = (z_1 - z_2)(t_+t_- + 1 - r_+r_-) + (z_1 + z_2)(r_+ - r-)$
$c = z_1z_2[-t_+t- + (1 + r_+)(1 + r_-)]$

Now simply inverting the above equations to find n in terms of t_+, r_+, t_- and r_-, and using the two relations,

$t_+ = e^{-ink_0d_s}[1 + r_+ - (1 - r_+)z_-/z_1](1 - z_-/z_2)^{-1}$
$t_+ = e^{ink_0d_s}[1 + r_+ - (1 - r_+)z_+/z_1](1 - z_+/z_2)^{-1}$

$$cos(nk_0d_s) = \frac{t_+}{2}[\frac{1 - z_-/z_2}{(1 + r_+ - (1 - r_+)z_-/z_1)} + \frac{(1 - z_-/z_2)}{(1 + r_+ - (1 - r_+)z_+/z_1)}] \tag{5.23}$$

This equation has many branches. After selecting the correct branch(which will be discussed later), we can proceed as follows to find the material parameters,

$$\epsilon = (n + i\xi)/z_+ \tag{5.24}$$

$$\mu = (n - i\xi)/z_+ \tag{5.25}$$

$$\xi = in(z_+ + z_-)(z_- - z_+)^{-1} \tag{5.26}$$

Thus it has successfully been shown to derive the effective parameter properties from the homogenized structure. In the next part, some basic application procedure of this method will be done and the difficulties faced will be discussed.

5.3 Application

5.3.1 Problems with matching Analytical and Simulational Caulculations

Now there are many problems that one faces while incorporating the numerically simulated values of reflectance, transmittance parameters obtained from COMSOL directly into these analytically derived equations as described above. These problems are addressed as follows.

Abnormal values of the effective parameters: - One of the foremost problem one faces when the raw S-parameter data are substituted in the equations is the abnormal high values of the effective parameters as shown below. These plots are just for a single thick layered structure.

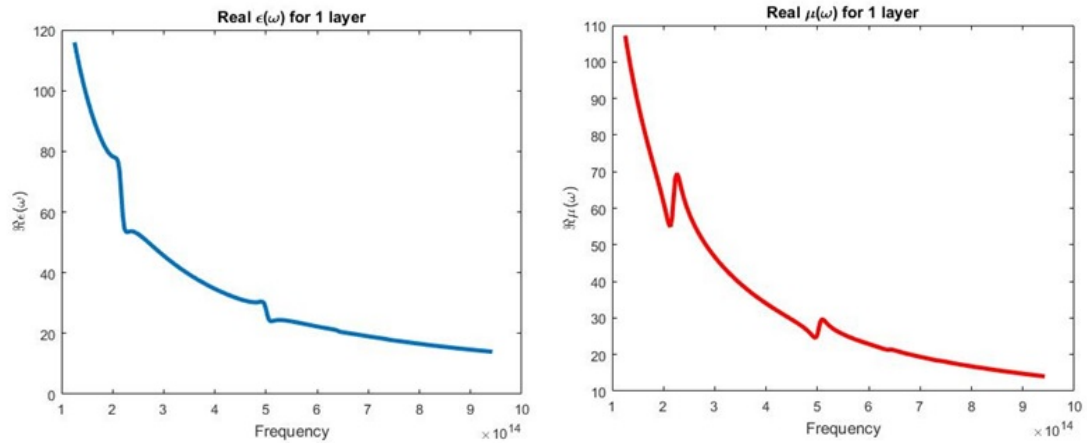

Figure 5.10: The electric and magnetic response before the corrections

This shows that $\epsilon(\omega)$ and $\mu(\omega)$ starts from an anomalous value which is not possible because the transmittance is near to 1 and the reflectance is near to zero at low frequencies which means that the epsilon and mu should start from or around unity instead. It is needless to mention here that the same abnormal behavior was observed when the number of layers were increased as well.

Resonance/Anti resonance coupling effect:- It is expected that when there is a resonance in Real of epsilon, a simultaneous resonance should also be observed in real of mu, although at other frequencies the electric and magnetic response should be independent

of each other. But as seen in the above figure, the reverse happens at the resonance frequencies- a peak in the μ is observed with a dip in the ϵ near 500 THz.

The third problem is selecting the *correct branch* of n as can be seen from the equation of n that it has an infinite number of branches. There are many existing robust methods for selecting the correct branch of n [44, 45]. But in this studied case, three simple things that should be kept in mind while selecting a branch are:-

i) the parameters $\epsilon(\omega)$,$\mu(\omega)$ and $\xi(\omega)$ shoule be continuous functions of frequency. Not only that their spectral derivatives should also be a continuous function.

ii)the branch should be selected in such a way that the real part of the impedance of the material should be greater than 0, otherwise the medium would be a gain medium and

iii)the sign convention makes it make sure that the imaginary part of n should always be less than zero, again for the same reason that, otherwise the wave will amplify while traveling through the medium.

5.3.2 Application to a Lossy Slab

For correcting the first two problems, a much simpler geometry is considered- a lossy dielectric slab structure is taken. The permittivity and permeability of this slab is assumed beforehand and based on these values we proceeded with the analytical calculations of the reflectance and transmittance coefficients. This structure will obviously have Fabry Perot refection, transmission effects now due to multiple reflections. With the normal Transfer Matrix Method Approach, the coefficients are calculated and compared with the numerical results for the basic geometry. The analytical calculations are shown in the supplemental pages.

Surprisingly, the modulus of the coefficients was found to be exactly equal as seen in the Figure5.12, but the phase is different. This led to the conclusion that there must be some extra phase gain or loss in the numerical simulations which makes the results different. This makes sense because in COMSOL one cannot directly take the port on the slab or on the material structure itself. The phase is from the analytical results and numerical results are compared and is shown in Figure(5.13) The port is kept at some distance and this leads to a phase gain when the wave travels that extra distance from the port to the material. So this phase gain has to be subtracted from the COMSOL

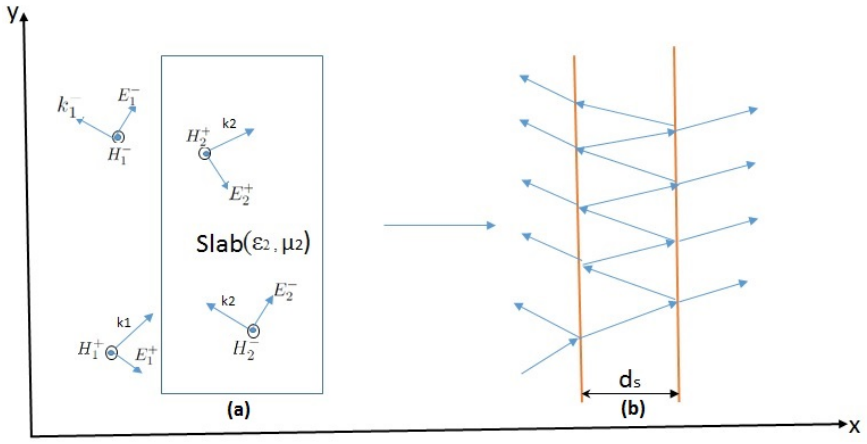

Figure 5.11: The geometry and the EM comfiguration of the Lossy Slab

coefficients and then included in the analytical equations. In simpler terms, it can be said that since the length of the unit cell is not the same in the two cases, there is some extraneous effects. There is also another possibility when the gain in phase can take place. Sometimes it might happen that the reflection, transmission coefficients are calculated with respect to the H-field in COMSOL while all the analytical calculations are done considering E-field. When both these factors are taken into account it is found that the phases perfectly overlap each other and the parameters that we started with for the slab is retrieved when put in the analytical equations and also the resonance problem is solved as well as can be seen in the later results. Therefore the problem is to substract the extra phase factors from the COMSOL parameters which is done and then the phase perfectly overlaps and the starting parameters are retrieved back. All the derivation for this slab is shown in the supplemental pages.

5.3.3 Application to the Graphene Split Ring Resonators

On applying the above correction methods to the layered graphene split ring resonator arrays, the following results are obtained.

Two interesting things to note here are - how after the phase correction the parameters start from unity. Moreover, as expected the permittivity of graphene is going negative at the resonance points implying typical metallic behavior. The most important thing

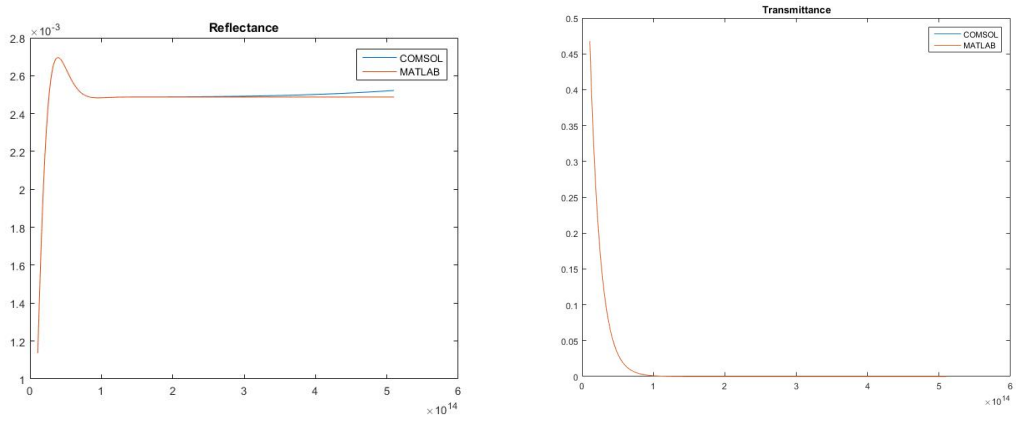

Figure 5.12: Analytical and numerical comparison of the Reflectance and Transmission coefficient

to note is that how the permeability in graphene is increasing with increasing number of layers. Initially for a single layer the medium behaves as a non-magnetic medium. But as the layers are increased the magnitude keeps on increasing. From mathematical point of view, it is expected as seen from the equation, because μ is directly proportional to the impedance. And impedance increases with increasing the layers and hence the wave suffers more attenuation which is directly proportional to exp(-kd). From physical point of view, it can be explained that when the layers are increased there is enhanced light matter interaction and the magnetic effects get pronounced. The bianisotropy or the magneto electric coupling is also very less which shows that the incident radiation finds it very hard to couple with the ring structure to show any appreciable magnetic effect.

5.3.4 Application to Gold Nanostructures

But things are different when one uses nanostructures made from gold. Similar procedure as before is applied. But here the Drude model is assumed for the conductivity in gold. The reflection, transmission, geometry and the effective parameters are shown respectively.

The magnetic effect,$\mu(\omega)$ in very pronounced in this structure and it is seen how it goes negative at the resonance points which one fails to observe in graphene. The reason

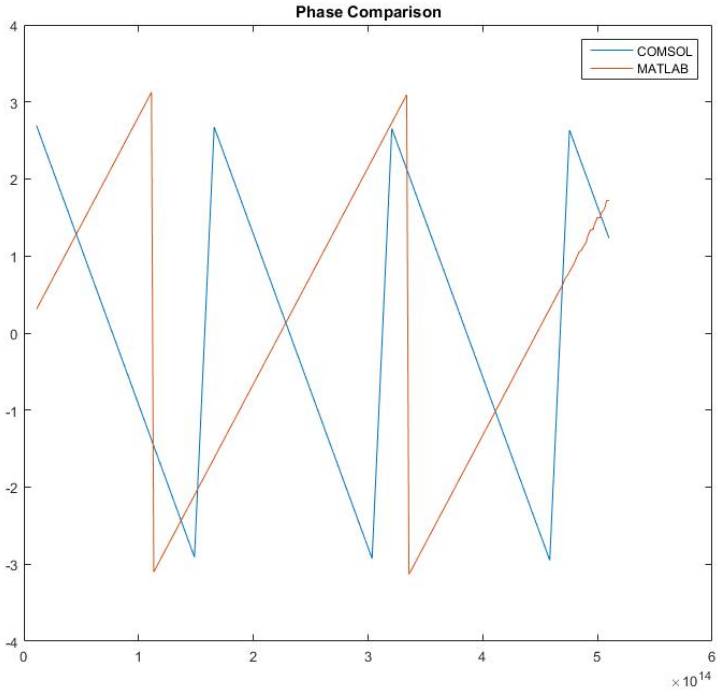

Figure 5.13: The Phase Difference

behind it is the high carrier concentration in gold particles at the same doping level of 0.5eV. This suggests strong plasmonics effects here. It can also be noticed as predicted that the bianisotropy factor is very large here as well which means that there is a strong electro magnetic coupling effect. Also another thing to notice is that although the $\mu(\omega)$ and $\epsilon(\omega)$ is going negative at some specific resonance points, but the refractive index does not go to less than zero at that point due to absence of chirality in the structure.

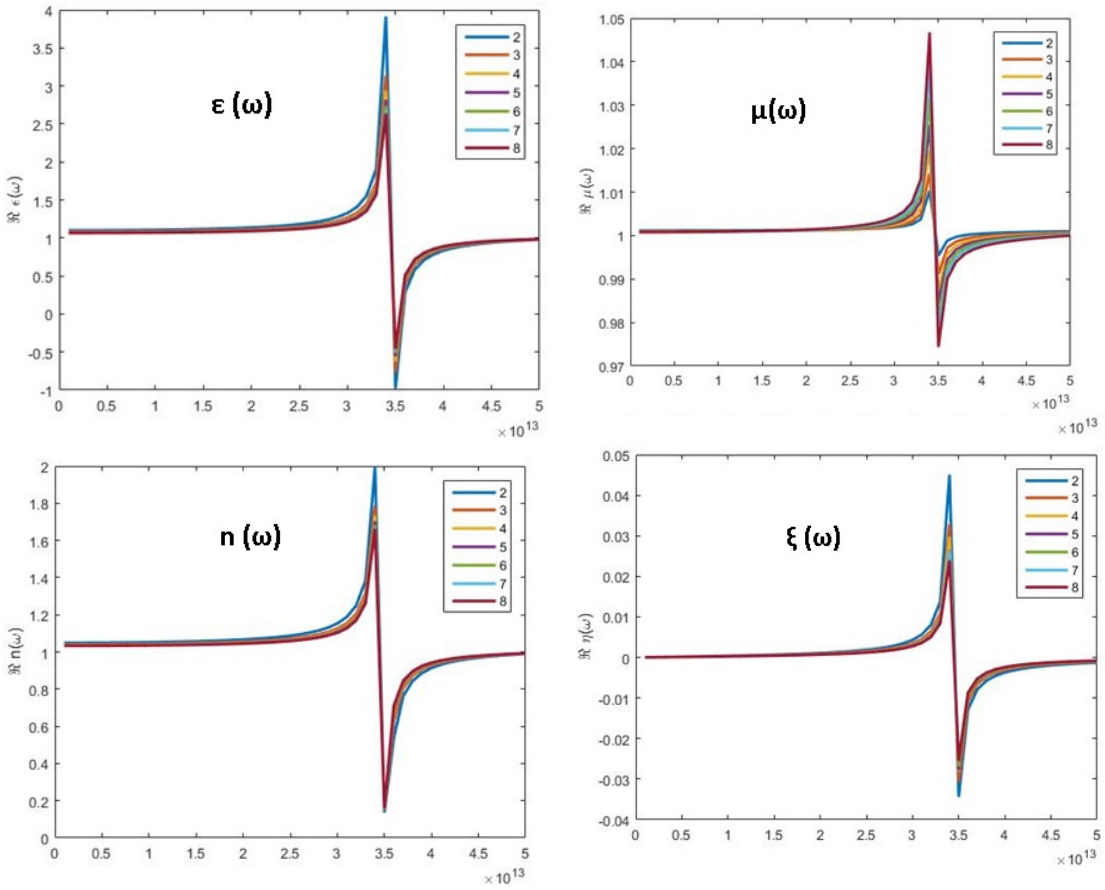

Figure 5.14: The Effective Parameter Derivations

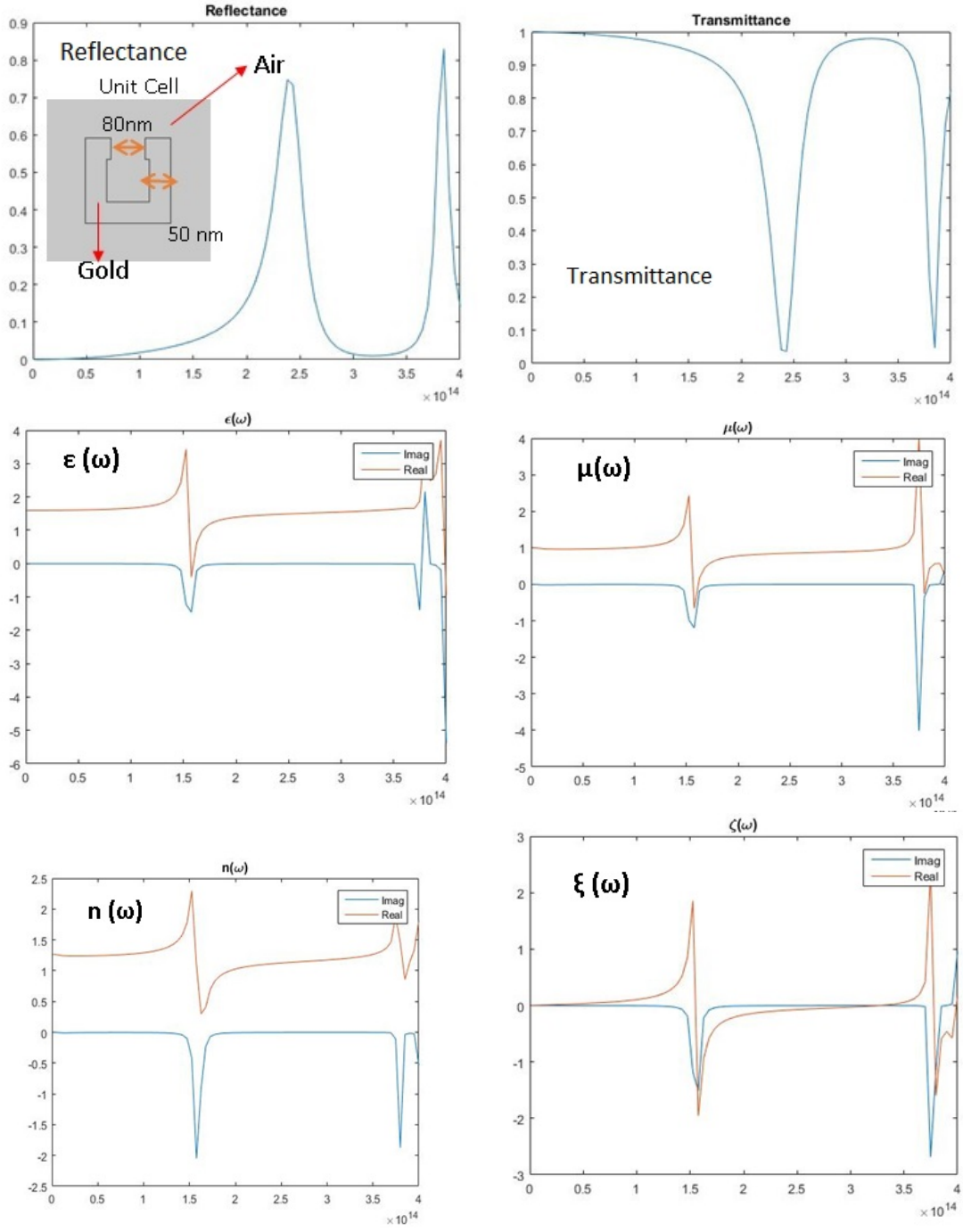

Figure 5.15: The Reflectance, Transmittance and the effective Parameters for Gold

Chapter 6

Summary

6.1 Conclusion

This section provides a summary of this thesis and also shares some of the future ideas that the author wishes to pursue in future. Arrays of split ring resonating structures made with graphene and gold is studied. At first the structure is homogenized and then the electromagnetic properties are measured for increasing number of layers. The main reason behind the study was to see whether one observes any magnetic effect from non magnetic materials or not. The split ring resonator structures, as predicted by Pendry and his group, makes a non magnetic material behaves as a magnetic material. It can be seen with the gold nano-structures. Although gold is itself a non magnetic material, but it shows magnetic effect when it is made into a split ring kind of structure and excited with the electromagnetic waves. The reason behind this effect can be attributed to the bianisotropic nature of the split ring structures which leads to the magneto electric coupling and thus a pronounced magnetic effect is observed. The simple derivations are shown in the earlier chapter. But the same effect cannot be observed with graphene split ring structures. In graphene the carrier concentration is much less for a doping of 0.5eV than in gold, hence the plasmonic behavior is not so pronounced which makes the material non magnetic. Thus it can be concluded that only those materials with a higher carrier concentration shows magnetic effect when made into these kind of resonating structures.

6.2 Future Work

Some future ideas that is thought of implementing considering the continuation of the above work are

i) Studying the magnetic effect with twisted bilayer graphene structure [46]

In twisted bilayer graphene structure, the centro-symmetric nature of the crystal is broken and chiral effects prevails in it. This effect gives an additional factor in the field equations along with the bianisotropic terms, which shows that magnetic effect can be produced due to three reasons:-the magnetic field itself of the incoming radiation, the bianisotropic factor resulting from the magneto-electric coupling and the chirality. Hence there can be a possibility of getting magnetic effects and a negative refractive index.

ii) The second idea is by using circularly polarized light or optical vortex beams on layered graphene structures. Optical vortex beams will produce circular dichroism in these structures, thus introducing chirality. Therefore, there is a chance of in-plane magnetic moment development because of the interlayer optical transitions.

iii) The third idea is to simply use other materials. Many 2D materials, beyond graphene have also been found recently. The idea is to use some other 2D materials like the metal dichalcogenides and black phosphorus and see the magnetic effect from these ring structures.

References

[1] Geim, Andre Konstantin. "Graphene: status and prospects." science 324.5934 (2009): 1530-1534.

[2] Novoselov, Kostya S., et al. "Electric field effect in atomically thin carbon films." science 306.5696 (2004): 666-669.

[3] Wallace, Philip Richard. "The band theory of graphite." Physical Review 71.9 (1947): 622.

[4] Boyle, W. S., and P. Nozires. "Band structure and infrared absorption of graphite." Physical Review 111.3 (1958): 782.

[5] Novoselov, K. S., et al. "Two-dimensional atomic crystals." Proceedings of the National Academy of Sciences of the United States of America 102.30 (2005): 10451-10453.

[6] Mermin, N. David. "Thermal properties of the inhomogeneous electron gas." Physical Review 137.5A (1965): A1441.

[7] Novoselov, K. S. A., et al. "Two-dimensional gas of massless Dirac fermions in graphene." nature 438.7065 (2005): 197-200.

[8] Falkovsky, L. A., and A. A. Varlamov. "Space-time dispersion of graphene conductivity." The European Physical Journal B 56.4 (2007): 281-284.

[9] Hwang, E. H., S. Adam, and S. Das Sarma. "Carrier transport in two-dimensional graphene layers." Physical review letters 98.18 (2007): 186806.

[10] Ziegler, K. "Minimal conductivity of graphene: Nonuniversal values from the Kubo formula." Physical Review B 75.23 (2007): 233407.

[11] Adam, Shaffique, et al. "A self-consistent theory for graphene transport." Proceedings of the National Academy of Sciences 104.47 (2007): 18392-18397.

[12] Adam, Shaffique, E. H. Hwang, and S. Das Sarma. "Scattering mechanisms and Boltzmann transport in graphene." Physica E: Low-dimensional Systems and Nanostructures 40.5 (2008): 1022-1025.

[13] Olsen, Thomas, et al. "Dispersive and covalent interactions between graphene and metal surfaces from the random phase approximation." Physical review letters 107.15 (2011): 156401.

[14] Cai, Jinming, et al. "Atomically precise bottom-up fabrication of graphene nanoribbons." Nature 466.7305 (2010): 470-473.

[15] Wakabayashi, Katsunori. "Electronic transport properties of nanographite ribbon junctions." Physical Review B 64.12 (2001): 125428.

[16] Low, Tony, and Phaedon Avouris. "Graphene plasmonics for terahertz to mid-infrared applications." ACS nano 8.2 (2014): 1086-1101.

[17] Ju, Long, et al. "Graphene plasmonics for tunable terahertz metamaterials." Nature nanotechnology 6.10 (2011): 630-634.

[18] Hwang, E. H., and S. Das Sarma. "Dielectric function, screening, and plasmons in two-dimensional graphene." Physical Review B 75.20 (2007): 205418.

[19] Yan, Hugen, et al. "Damping pathways of mid-infrared plasmons in graphene nanostructures." Nature Photonics 7.5 (2013): 394-399.

[20] Nikitin, A. Yu, et al. "Surface plasmon enhanced absorption and suppressed transmission in periodic arrays of graphene ribbons." Physical Review B 85.8 (2012): 081405.

[21] Mikhailov, Sergey A., and N. A. Savostianova. "Microwave response of a two-dimensional electron stripe." Physical Review B 71.3 (2005): 035320.

[22] Prodan, E., et al. "A hybridization model for the plasmon response of complex nanostructures." Science 302.5644 (2003): 419-422.

[23] Davis, T. J., D. E. Gmez, and K. C. Vernon. "Simple model for the hybridization of surface plasmon resonances in metallic nanoparticles." Nano letters 10.7 (2010): 2618-2625.

[24] Yao, B. M., et al. "Experimental realization of negative refraction using one metasurface." Applied Physics Letters 106.12 (2015): 121903.

[25] Shchelokova, Alena V., et al. "Experimental realization of invisibility cloaking." Physics-Uspekhi 58.2 (2015): 167.

[26] Pendry, John Brian. "Negative refraction makes a perfect lens." Physical review letters 85.18 (2000): 3966.

[27] Plasmonics, SA Maier. "fundamentals and Applications." Springer Science+ Business Media 200 (2007): 224.

[28] Veselago, Viktor G. "The electrodynamics of substances with simultaneously negative values of and?." Soviet physics uspekhi 10.4 (1968): 509.

[29] Pendry, J. B., et al. "Extremely low frequency plasmons in metallic mesostructures." Physical review letters 76.25 (1996): 4773.

[30] Pendry, John B., et al. "Magnetism from conductors and enhanced nonlinear phenomena." IEEE transactions on microwave theory and techniques 47.11 (1999): 2075-2084.

[31] Smith, David R., et al. "Composite medium with simultaneously negative permeability and permittivity." Physical review letters 84.18 (2000): 4184.

[32] Paul, Oliver, et al. "Negative index bulk metamaterial at terahertz frequencies." Optics express 16.9 (2008): 6736-6744.

[33] Ramakrishna, S. Anantha. "Physics of negative refractive index materials." Reports on Progress in Physics 68.2 (2005): 449.

[34] Zhou, Jiangfeng, et al. "Negative refractive index due to chirality." Physical Review B 79.12 (2009): 121104.

[35] Zambrana-Puyalto, Xavier, Xavier Vidal, and Gabriel Molina-Terriza. "Angular momentum-induced circular dichroism in non-chiral nanostructures." Nature communications 5 (2014).

[36] Katsarakis, N., et al. "Electric coupling to the magnetic resonance of split ring resonators." Applied Physics Letters 84.15 (2004): 2943-2945.

[37] Albooyeh, M., et al. "Revisiting substrate-induced bianisotropy in metasurfaces." Physical Review B 91.19 (2015): 195304.

[38] Kraft, Matthias, et al. "Bianisotropy and magnetism in plasmonic gratings." ACS Photonics 3.5 (2016): 764-769.

[39] Mackay, Tom G. Electromagnetic anisotropy and bianisotropy: a field guide. World Scientific, 2010.

[40] Smith, David R., and John B. Pendry. "Homogenization of metamaterials by field averaging." JOSA B 23.3 (2006): 391-403.

[41] Chen, Hongsheng, et al. "Equivalent circuit model for left-handed metamaterials." Journal of applied physics 100.2 (2006): 024915.

[42] Smith, D. R., et al. "Determination of effective permittivity and permeability of metamaterials from reflection and transmission coefficients." Physical Review B 65.19 (2002): 195104.

[43] Kriegler, Christine Eliane, et al. "Bianisotropic photonic metamaterials." IEEE journal of selected topics in quantum electronics 16.2 (2010): 367-375.

[44] Chen, Xudong, et al. "Robust method to retrieve the constitutive effective parameters of metamaterials." Physical Review E 70.1 (2004): 016608.

[45] Chen, Lei, et al. "Determining the effective electromagnetic parameters of bianisotropic metamaterials with periodic structures." Progress In Electromagnetics Research M 29 (2013): 79-93.

[46] Lu, Chih-Pin, et al. "Local and global screening properties of graphene revealed through Landau level spectroscopy." arXiv preprint arXiv:1504.07540 (2015).

Appendix A

Supplemental Calculations

A.1 The Lossy Slab

Inside the medium Field Equations : Finding k_1

The basic equations:-

$\nabla \times \vec{E} = -\frac{\partial \vec{B}}{\partial t}$ .....(1) and

$\nabla \times \vec{H} = \frac{\partial \vec{D}}{\partial t}$.....(2)[considering current free region]

The external fields: $\vec{E} = Ee^{(i\omega t - ik_1 z)}\hat{\mathbf{x}}$ and $\vec{H} = He^{(i\omega t - ik_1 z)}\hat{\mathbf{y}}$

while inside the medium the fields are $\vec{D} = \epsilon_o \epsilon_{r1}\vec{E}$ and $\vec{B} = \mu_0 \mu_{r1}\vec{H}$ where, ϵ_{r1} and μ_{r1} are the relative permittivity and permeability inside the medium. Therefore $\epsilon_1 = \epsilon_0 \epsilon_{r1}$ and $\mu_1 = \mu_0 \mu_{r1}$

Taking curl of equation (1),

$\nabla \times \nabla \times \vec{E} = -\frac{\partial(\nabla \times \vec{B})}{\partial t}$

$\nabla(\nabla.\vec{E}) - \nabla^2 \vec{E} = -\mu_0 \mu_{r1} \frac{\partial(\nabla \times \vec{H})}{\partial t}$

The medium is source free, which means $\nabla.\vec{E} = 0$ and by using Equation 2 implies, $\nabla^2 \vec{E} = \mu_0 \mu_{r1} \frac{\partial}{\partial t}[\frac{\partial \vec{D}}{\partial t}]$,

or, $\nabla^2 \vec{E} = \mu_0 \epsilon_0 \mu_{r1} \epsilon_{r1} \frac{\partial^2 \vec{E}}{\partial t}$,

Now substituting the simple plane wave equation for $\vec{E}$,

we can express the left hand side,
$\nabla^2\vec{E} = (\frac{\partial^2}{\partial x^2} + \frac{\partial^2}{\partial y^2} + \frac{\partial^2}{\partial z^2})\vec{E} = (-ik_1).(-ik_1)\vec{E} = -k_1^2\vec{E}$
implies,
$\nabla^2\vec{E} = -k_1^2\vec{E} = -\epsilon_0\mu_0\epsilon_{r1}\mu_{r1}\omega^2\vec{E}$
or, $k_1^2 = \epsilon_1\mu_1\omega^2$
or, $\Rightarrow \boxed{k_1 = \pm\omega\sqrt{\mu_1\epsilon_1}}$

The new wave equations in the medium in terms of incident and reflected wave

$\vec{E}^i = E^i e^{i\omega t}e^{-ik_1 z}\hat{\mathbf{x}}$ where k_1 is as defined in the above boxed equation.
Similarly, $\vec{H}^i = H^i e^{-ik_1 z}e^{i\omega t}\hat{\mathbf{y}}$
Therefore substituting this new form in equation (2),
that is, $\nabla \times \vec{H}^i = ik_1 H^i\hat{y} = \frac{\partial\vec{D}^i}{\partial t} = \epsilon_1\frac{\partial\vec{E}^i}{\partial t}$, we get,

$$\boxed{\omega\epsilon_1 E^i = k_1 H^i}$$

Similarly for the reflected wave from the interface $\vec{E}^r$ and $\vec{H}^r$ we have ,

$$\boxed{\omega\epsilon_1 E^r = -k_1 H^r}$$

Finding the Reflection coefficient and Transmission coefficient :TM polarization

Applying the **boundary condition** for normal incidence that the components of electric and magnetic field parallel to the **interface** are equal,
we have $H^i + H^r = H^t$
and $E^i + E^r = E^t$

Substituting the values of E in the above equation in terms of H,
we get, $\frac{k_1}{\omega\epsilon_1}[H^i - H^r] = \frac{k_2}{\omega\epsilon_2}E^t$
or, $[1 - r] = \frac{\epsilon_1 k_2}{\epsilon_2 k_1}t$

where $r = H^r/H^i$ and $t = H^t/H^i$

Again from $E^i + E^r = E^t$,
we have, $1 + r = t$
Thus solving the two equations,
we have $\boxed{r = \frac{\epsilon_2 k_1 - \epsilon_1 k_2}{\epsilon_2 k_1 + \epsilon_1 k_2}}$

and $\boxed{t = \frac{2\epsilon_2 k_1}{\epsilon_2 k_1 + \epsilon_1 k_2}}$ In the above equation the transmission coefficient t is multiplied by a factor of $x = \sqrt{\frac{\mu_2 \epsilon_1}{\mu_1 \epsilon_2}}$ so that $|T|^2 + |R|^2 = 1$

Finding the Reflection coefficient and Transmission coefficient :TE polarization

The external fields: $\vec{E} = Ee^{(i\omega t - ik_1 z)}\hat{\mathbf{y}}$ and $\vec{H} = He^{(i\omega t - ik_1 z)}\hat{\mathbf{x}}$
while inside the medium the fields are $\vec{D} = \epsilon_o \epsilon_{r1}\vec{E}$ and $\vec{B} = \mu_0 \mu_{r1}\vec{H}$
Substituting this form in equation 1, that is ,
$\nabla \times \vec{E} = -\frac{\partial \vec{B}}{\partial t}$ we have, for incident and reflected waves,
$\boxed{\mu_1 \omega H^i = -k_1 E^i \text{ and } \mu_1 \omega H^r = k_1 E^r}$.....(3)

Now applying the same **boundary conditions** as before that the electric field and magnetic field is **parallel** to the interface,
we have, $E^i + E^r = E^t$
and $H^i + H^r = H^t$
or, $-\frac{k_1}{\omega\mu_1}E^i + \frac{k_1}{\omega\mu_1}E^r = -\frac{k_2}{\omega\mu_2}E^t$
or, $[1 - r] = \frac{\mu_1 k_2}{\mu_2 k_1}t$, where $r = E^r/E^i$ and $t = E^t/E^i$ Solving the above equations
we have, $\boxed{r = \frac{\mu_2 k_1 - \mu_1 k_2}{\mu_2 k_1 + \mu_1 k_2}}$

and $\boxed{t = \frac{2\mu_2 k_1}{\mu_2 k_1 + \mu_1 k_2}}$ [DERIVED]

Reflection, Transmission coefficient formula for a thin dielectric slab due

to multiple scattering inside

Considering now a slab of thickness d_s with permittivity and permeability ϵ_2 and μ_2 respectively, immersed in between two semi infinite media (ϵ_1, μ_1) and (ϵ_2, μ_2) the reflection and transmission coefficients are calculated as shown in Figure . In this case, the boundary condition for the TM polarization will be modified as follows:-

we have $H_1^+ + H_1^- = H_2^+ + H_2^-$

and $E_{1y}^+ + E_{1y}^- = E_{2y}^+ + E_{2y}^-$

Similarly using the same approach as before that is representing E in terms of H as $\frac{\epsilon_{1,2}\omega}{c} E_{1y,2y}^{\pm} = \pm k_{1,2} H_{1,2}^{\pm}$, we get the following relationship,

$$\begin{bmatrix} 1 & 1 \\ \frac{k_{1z}}{\epsilon_1} & -\frac{k_{1z}}{\epsilon_1} \end{bmatrix} \times \begin{bmatrix} H_1^+ \\ H_1^- \end{bmatrix} = \begin{bmatrix} 1 & 1 \\ -\frac{k_{2z}}{\epsilon_2} & \frac{k_{2z}}{\epsilon_2} \end{bmatrix} \times \begin{bmatrix} H_2^+ \\ H_2^- \end{bmatrix}$$

which can be re-written as $\begin{bmatrix} H_2^+ \\ H_2^+ \end{bmatrix} = \mathbf{M}_{12} \begin{bmatrix} H_1^+ \\ H_1^+ \end{bmatrix}$

where $\mathbf{M}_{12} = \begin{bmatrix} 1 + \frac{\epsilon_2 k_{1z}}{\epsilon_1 k_{2z}} & 1 - \frac{\epsilon_2 k_1}{\epsilon_1 k_2} \\ 1 - \frac{\epsilon_2 k_1}{\epsilon_1 k_2} & 1 + \frac{\epsilon_2 k_1}{\epsilon_1 k_2} \end{bmatrix}$

Now simple transfer matrix approach is used to find the propagation through the slab as below:

$$\begin{bmatrix} H_2^+ \\ H_2^+ \end{bmatrix} = \mathbf{M}_{12} \begin{bmatrix} e^{ik_2 d_s} & 0 \\ 0 & e^{-ik_2 d_s} \end{bmatrix} \mathbf{M}_{23} \begin{bmatrix} H_1^+ \\ H_1^+ \end{bmatrix}$$

which can be written as $\begin{bmatrix} H_2^+ \\ H_2^+ \end{bmatrix} = \mathbf{M}_{slab} \begin{bmatrix} H_1^+ \\ H_1^+ \end{bmatrix}$,

where $\mathbf{M}_{slab} = \mathbf{M}_{12} \times \begin{bmatrix} e^{ik_2 d_s} & 0 \\ 0 & e^{-ik_2 d_s} \end{bmatrix} \times \mathbf{M}_{23}$ and each of the elements of the M_{slab} is given as below:-

$$\mathrm{M}_{slab}^{11} = \tfrac{1}{2}[1 + \tfrac{\epsilon_3 k_1}{\epsilon_1 k3}] cos(k_2 d_s) + \tfrac{i}{2}[\tfrac{\epsilon_3 k_2}{\epsilon_2 k_3} + \tfrac{\epsilon_2 k_1}{\epsilon_1 k_2}] sin(k_2 d_s)$$

$$\mathrm{M}_{slab}^{12} = \tfrac{1}{2}[1 - \tfrac{\epsilon_3 k_1}{\epsilon_1 k3}] cos(k_2 d_s) + \tfrac{i}{2}[\tfrac{\epsilon_3 k_2}{\epsilon_2 k_3} - \tfrac{\epsilon_2 k_1}{\epsilon_1 k_2}] sin(k_2 d_s)$$

$M^{21}_{slab} = \frac{1}{2}[1 - \frac{\epsilon_3 k_1}{\epsilon_1 k3}]cos(k_2 d_s) - \frac{i}{2}[\frac{\epsilon_3 k_2}{\epsilon_2 k_3} - \frac{\epsilon_2 k_1}{\epsilon_1 k_2}]sin(k_2 d_s)$ and

$M^{22}_{slab} = \frac{1}{2}[1 + \frac{\epsilon_3 k_1}{\epsilon_1 k3}]cos(k_2 d_s) - \frac{i}{2}[\frac{\epsilon_3 k_2}{\epsilon_2 k_3} + \frac{\epsilon_2 k_1}{\epsilon_1 k_2}]sin(k_2 d_s)$
where r_+ = reflectance from the positive side = $-\frac{M_{21}}{M_{22}}$ and
t_+ = transmittance from the positive side = $\frac{det(M)}{M_2 2}$

A.2 Graphene Nanoribbons Surface Plasmons

The incident Electric and Magnetic field for the two mediums i=1 and 2c can be taken for the TM mode as:-

$$E = (E_{ix}, 0, E_{iz})e^{(iqx - K_i z - i\omega t)}\hat{z} \quad and \tag{A.1}$$

$$H = (0, H_{iy}, o)e^{(iqx - K_i z - i\omega t)}\hat{y} \tag{A.2}$$

Therefore substituting the above two equations in the two Maxwell's equations

$$\nabla \times E = -\frac{\partial B}{\partial t} \tag{A.3}$$

$$\nabla \times H = -\frac{\partial D}{\partial t} \tag{A.4}$$

one gets,

$$-K_1 E_{1x} - iqE_{1z} = i\omega B_{1y} \tag{A.5}$$

$$-K_2 E_{1x} - iqE_{2z} = i\omega B_{2y} \tag{A.6}$$

and

$$-K_1 B_{1y} = -\frac{i\omega}{c^2}\epsilon_1 E_{1x} \tag{A.7}$$

$$-K_2 B_{2y} = -\frac{i\omega}{c^2}\epsilon_2 E_{2x} \tag{A.8}$$

Now rearranging the equations 9,10,11 and 12,

$$qB_{2y} = -\frac{\omega}{c^2}\epsilon_2 E_{2z} \tag{A.9}$$

$$qb_{1y} = -\frac{\omega}{c^2}\epsilon_1 E_{1z} \tag{A.10}$$

Thus rearranging and substituting the above equations, one obtains the dispersion relations for each medium as

$$K_1^2 = q^2 - \omega^2\epsilon_1/c^2 \tag{A.11}$$

$$K_2^2 = q^2 - \omega^2\epsilon_2/c^2 \tag{A.12}$$

Now applying, $E_{1t} = E_{2t}$,
and $H_{1t} - H_{2t} = \sigma\hat{n}E_1$
$\implies E_{1x} = E_{2x}$
and $B_{1y} - B_{2y} = -\sigma E_{1x}$
Substituting for E, one gets
$1 + \frac{K_1\epsilon_2}{K_2\epsilon_1} + i\sigma\frac{K_1}{\epsilon_0\omega\epsilon_1} = 0$

$$\boxed{\frac{\epsilon_1}{K_1} + \frac{\epsilon_2}{K_2} + i\frac{\sigma}{\omega\epsilon_0} = 0} \tag{A.13}$$

Therefore, substituting for K_1 and K_2 from equations 15 and 16, the final dispersion relation is,

$$\boxed{\frac{\epsilon_1}{\sqrt{q^2 - \frac{\omega^2\epsilon_1}{c^2}}} + \frac{\epsilon_2}{\sqrt{q^2 - \frac{\omega^2\epsilon_1}{c^2}}} = -i\frac{\sigma}{\omega\epsilon_0}} \tag{A.14}$$

Now in the non retarded regime when $q >> \omega/c$, equation 18 becomes
$\frac{\epsilon_1+\epsilon_2}{q} = -i\frac{\sigma}{\omega\epsilon_0}$ or,

$$\boxed{q \approx \epsilon_0\frac{\epsilon_{r1} + \epsilon_{r2}}{2} \times \frac{2i\omega}{\sigma(\omega.q)}} \tag{A.15}$$

A.3 Finding f(k) - the Structural Factor

$$K.\vec{\delta_1} = \frac{1}{3}\frac{2\pi}{a}l\sqrt{3} = \frac{2\pi}{3}$$

$$K.\vec{\delta_2} = \frac{1}{3}\frac{2\pi}{a}l(-\sqrt{3}/2 + \sqrt{3}/2) = 0$$

$$K.\vec{\delta_3} = \frac{1}{3}\frac{2\pi}{a}l(-\sqrt{3}/2 - \sqrt{3}/2 = -\frac{2\pi}{3}$$

Thus substituting in f(k) equation,

$$\begin{aligned} f(k) &= exp(+iK.\vec{\delta_1}) + exp(K.\vec{\delta_2} + K.\vec{\delta_3}) \\ &= exp(+i\frac{2\pi}{3}) + exp(i0) + exp(-i\frac{2\pi}{3}) \\ &= -1/2 + i\sqrt{3}/2 + 1 - 1/2 - i\sqrt{2}/2 \end{aligned}$$

which is equal to $= 0$

A.4 Finding the elements of the Hamiltonian Matrix

$$\begin{aligned} f(\vec{q}) &= \vec{q}\nabla_k f|_{\vec{K}} \\ &= \vec{q}[\delta_1 exp(+iK.\vec{\delta_1}) + exp(K.\vec{\delta_2} + K.\vec{\delta_3})] \end{aligned}$$

$$= l \begin{bmatrix} q_x \\ q_y \end{bmatrix} \begin{bmatrix} 1 \\ 0 \end{bmatrix} (-1/2 + i\sqrt{3}/2) + \begin{bmatrix} q_x \\ q_y \end{bmatrix} l \begin{bmatrix} -1/2 \\ \sqrt{3}/2 \end{bmatrix} + l \begin{bmatrix} -1/2 \\ -\sqrt{3}/2 \end{bmatrix} (-1/2 - i\sqrt{3}/2)$$

=

$$l \begin{bmatrix} q_x \\ q_y \end{bmatrix} \begin{bmatrix} -3/4 + i3\sqrt{3}/4 \\ i3\sqrt{3}/4 - 3/4 \end{bmatrix} \tag{A.16}$$

=

$$\boxed{\frac{3l}{2}(q_x - iq_y)e^{i\theta}} \tag{A.17}$$